Atmos. Chem. Phys. Discuss., 12, 21713–21778, 2012
www.atmos-chem-phys-discuss.net/12/21713/2012/
doi:10.5194/acpd-12-21713-2012

Atmospheric Chemistry and Physics Discussions

Evaluation of preindustrial to present-day black carbon and its albedo forcing from ACCMIP (Atmospheric Chemistry and Climate Model Intercomparison Project)

Y. H. Lee[1], J.-F. Lamarque[2], M. G. Flanner[3], C. Jiao[3], D. T. Shindell[1], T. Berntsen[4], M. M. Bisiaux[5], J. Cao[6], W. J. Collins[7], M. Curran[8], R. Edwards[9], G. Faluvegi[1], S. Ghan[10], L. W. Horowitz[11], J. R. McConnell[5], G. Myhre[12], T. Nagashima[13], V. Naik[14], S. T. Rumbold[7], R. B. Skeie[13], K. Sudo[15], T. Takemura[16], and F. Thevenon[17]

[1]NASA Goddard Institute for Space Studies and Columbia Earth Institute, New York, NY, USA
[2]National Center for Atmospheric Research (NCAR), Boulder, CO, USA
[3]Department of Atmospheric, Oceanic and Space Sciences, University of Michigan, Ann Arbor, MI, USA
[4]Center for International Climate and Environmental Research Oslo (CICERO) and Department of Geosciences, University of Oslo, Oslo, Norway
[5]Desert Research Institute, Nevada System of Higher Education, Reno, NV, USA
[6]State Key Laboratory of Loess and Quaternary Geology, Institute of Earth Environment, Chinese Academy of Sciences, Xi'an, China

[7]Met Office, Hadley Centre, Exeter, UK
[8]Department of the Environment and Heritage, Australian Antarctic Division, Antarctic Climate and Ecosystem Cooperative Research Centre, Tasmania, Australia
[9]Department of Imaging and Applied Physics, Curtin University, Bentley, WA, Australia
[10]Pacific Northwest National Laboratory, Richland, WA, USA
[11]NOAA Geophysical Fluid Dynamics Laboratory, Princeton, NJ, USA
[12]Center for International Climate and Environmental Research Oslo (CICERO), Oslo, Norway
[13]National Institute for Environmental Studies, Tsukuba-shi, Ibaraki, Japan
[14]UCAR/NOAA Geophysical Fluid Dynamics Laboratory, Princeton, NJ, USA
[15]Department of Earth and Environmental Science, Graduate School of Environmental Studies, Nagoya University, Nagoya, Japan
[16]Research Institute for Applied Mechanics, Kyushu University, Fukuoka, Japan
[17]F.-A. Forel Institute, University of Geneva, Versoix, Switzerland

Received: 26 July 2012 – Accepted: 10 August 2012 – Published: 23 August 2012

Correspondence to: Y. H. Lee (yunha.lee@nasa.gov)

Published by Copernicus Publications on behalf of the European Geosciences Union.

ACPD
12, 21713–21778, 2012

Abstract

As part of the Atmospheric Chemistry and Climate Model Intercomparison Project (ACCMIP), we evaluate the historical black carbon (BC) aerosols simulated by 8 ACCMIP models against observations including 12 ice core records, long-term surface mass concentrations and recent Arctic BC snowpack measurements. We also estimate BC albedo forcing by performing additional simulations using offline models with prescribed meteorology from 1996–2000. We evaluated the vertical profile of BC snow concentrations from these offline simulations using the recent BC snowpack measurements.

Despite using the same BC emissions, the global BC burden differs by approximately a factor of 3 among models due to differences in aerosol removal parameterizations and simulated meteorology: 34 Gg to 103 Gg in 1850 and 82 Gg to 315 Gg in 2000. However, the global BC burden from preindustrial to present-day increases by 2.5–3 times with little variation among models, roughly matching the 2.5-fold increase in total BC emissions during the same period. We find a large divergence among models at both Northern Hemisphere (NH) and Southern Hemisphere (SH) high latitude regions for BC burden and at SH high latitude regions for deposition fluxes. The ACCMIP simulations match the observed BC surface mass concentrations well in Europe and North America except at Jungfraujoch and Ispra. However, the models fail to predict the Arctic BC seasonality due to severe underestimations during winter and spring. The simulated vertically resolved BC snow concentrations are, on average, within a factor of 2–3 of the BC snowpack measurements except for Greenland and the Arctic Ocean.

For the ice core evaluation, models tend to capture both the observed temporal trends and the magnitudes well at Greenland sites. However, models fail to predict the decreasing trend of BC depositions/ice-core concentrations from the 1950s to the 1970s in most Tibetan Plateau ice cores. The distinct temporal trend at the Tibetan Plateau ice cores indicates a strong influence from Western Europe, but the modeled BC increases in that period are consistent with the emission changes in Eastern Europe, the Middle East, South and East Asia. At the Alps site, the simulated BC suggests

ACPD
12, 21713–21778, 2012

a strong influence from Europe, which agrees with the Alps ice core observations. Models successfully simulate higher BC concentrations observed at Zuoqiupu during the non-monsoon season than monsoon season, but models underpredict BC in both seasons. Despite a large divergence in BC deposition at two Antarctic ice core sites, models are able to capture the relative increase from preindustrial to present-day seen in the ice cores.

In 2000 relative to 1850, globally annually averaged BC surface albedo forcing from the offline simulations ranges from 0.014 to 0.019 $W m^{-2}$ among the ACCMIP models. Comparing offline and online BC albedo forcings computed by some of the same models, we find that the global annual mean can vary by up to a factor of two because of different aerosol models or different BC-snow parameterizations and snow cover. The spatial distributions of the offline BC albedo forcing in 2000 show especially high BC forcing (i.e. over 0.1 $W m^{-2}$) over Manchuria, Karakoram, and most of the Former USSR. Models predict the highest global annual mean BC forcing in 1980 rather than 2000, mostly driven by the high fossil fuel and biofuel emissions in the Former USSR in 1980.

1 Introduction

Black carbon (BC) is the light-absorbing portion of carbonaceous aerosols that is emitted through the incomplete combustion of fossil fuel, biofuel, and biomass. BC aerosols influence climate in the following ways: (1) BC absorbs and scatters radiation, mainly resulting in warming the atmosphere and reducing solar radiation reaching the surface of Earth, which is known as aerosol direct effect. (2) The direct effect of BC can affect cloud formation by changing the atmospheric stability and/or relative humidity ("semi-direct effect") (e.g. Ackerman et al., 2000; Koch and Del Genio, 2010). (3) BC can alter Cloud Condensation Nuclei (CCN) concentrations and cloud properties when internally mixed with hydrophilic aerosols such as sulfate, which is known as aerosol indirect effect. BC can also affect the ice and mixed-phase clouds by acting as ice nuclei

ACPD
12, 21713–21778, 2012

(e.g. Cozic et al., 2007, 2008). (4) BC reduces the surface albedo when deposited in and on snow and ice surfaces, which is called as BC albedo effect (e.g. Hansen and Nazarenko, 2004; Jacobson, 2004).

Areas covered with snow or ice surface (e.g. the Arctic, the Antarctic, high mountain regions, Northern Canada and Northern Eurasia) are particularly sensitive to global climate change and have undergone rapid changes in recent decades (e.g. Lubin and Vogelmann, 2006; Kehrwald et al., 2008; Xu et al., 2009b). The radiative effects of BC particles are important in these regions even at relatively low concentrations because of its dominant light absorbing properties. The BC albedo effect can be especially important because not only does it darken the surface but can also this cause a further warming as it initiates the snow albedo feedback by promoting snow melting (e.g. Flanner et al., 2007, 2009). Reduction of BC emissions has been seriously considered as a potential method for mitigation of a global warming trend especially over the Arctic and Tibet Plateau (e.g. Quinn et al., 2008; Kopp and Mauzerall, 2010).

To understand BC impacts on climate in these climatically-vulnerable regions, a number of BC measurements have been conducted, including surface mass concentrations (e.g. Collaud Coen et al., 2007; Chaubey et al., 2010; Gong et al., 2010; Andrew et al., 2011), BC in snow (e.g. Doherty et al., 2010; Hegg et al., 2010; Yasunari et al., 2010), and BC in ice cores (e.g. McConnell et al., 2007; Ming et al., 2008; Xu et al., 2009a; Bisiaux et al., 2012b). These BC measurements are based on either optical or thermal-optical methods (e.g. Moosmuller et al., 2009); thermal methods measure the refractory portion of total carbon, which is therefore called elemental carbon (EC) instead of BC. Filter-based optical instruments such as Particle Soot Absorption Photometer (PSAP) and Aethalometer have been frequently used in long-term atmospheric sampling networks (e.g. Bodhaine, 1995; Sharma et al., 2004) because of ease of remote operation. These instruments measure a light absorption coefficient that is converted to BC mass concentrations by assuming a mass absorption cross section and therefore provide an "equivalent BC (EBC)" concentration since this is not a direct measurement of BC. The EBC concentration can suffer from using an improper mass absorption

ACPD
12, 21713–21778, 2012

cross section that is highly influenced by the aerosol mixing state and other light absorbing species such as organic matter and mineral dust (e.g. Sharma et al., 2002). Also interferences caused by scattering aerosols on the filter can lead to artificial high absorption (e.g. Sharma et al., 2002). Thermal-optical techniques have been used to measure BC mass in snow to investigate BC transport to the Arctic and BC albedo effect (Doherty et al., 2010). This can be also affected by the same conversion problems as described above.

As previously mentioned, BC (measured with optical methods) is rather distinct from EC (measured with thermal methods) and BC and EC concentrations can differ by a factor of 3–4 depending on the aerosol characteristics (Reisinger et al., 2008) and up to a factor of 7 (Watson et al., 2005). However, most aerosol models tend to use the term BC, EC, or soot interchangeably (Vignati et al., 2010). It is difficult to clearly distinguish these terminologies in a model because emission, physical, chemical, and optical properties used in a model are built/chosen based on various observation sources. Importantly, BC emission inventories are largely based on EC data.

There have been numerous modeling studies to understand BC source attribution and to estimate its climate impact. Many studies have focused on the Arctic including Greenland (e.g. Koch and Hansen, 2005; Stohl, 2006; Law and Stohl, 2007; Shindell et al., 2008; Hirdman et al., 2010a,b; Huang et al., 2010a; Jacobson, 2010; Warneke et al., 2010). These studies consistently show that Eurasia and North American BC emissions contribute significantly to Arctic BC, while Hirdman et al. (2010b) demonstrate the importance of the Arctic BC emissions to the Arctic BC concentrations. Law and Stohl (2007) and Hirdman et al. (2010b) point out that, compared to the rest of Arctic, Greenland is more influenced by BC originating from southeast Asia and North America due to its high topography. To inter-compare BC models, Koch et al. (2009b) evaluated several BC models with available observations including surface mass concentrations, aircraft measurements, aerosol absorption optical depth from AERONET and Ozone Monitoring Instruments, and BC column estimations based on AERONET under the AeroCom model intercomparison project. Shindell et al. (2008) investigated

ACPD
12, 21713–21778, 2012

transport of BC emitted from each continent to the Arctic under the Hemispheric Transport of Air Pollution (HTAP) project. Unlike the Arctic, only a few modeling studies have focused on the Tibetan Plateau (Kopacz et al., 2011; Lu et al., 2012), the Alps (Fagerli et al., 2007), and the Antarctic (Graf et al., 2010). The two modeling studies on the Tibetan Plateau find BC transported from South Asia and East Asia are major sources, although the relative contributions of each source region vary with seasons and the receptor location.

As part of the Atmospheric Chemistry and Climate Model Intercomparison Project (ACCMIP; Lamarque et al., 2012a), our primary goal in this paper is to evaluate preindustrial to present-day BC in ACCMIP models with ice cores sampled from the Arctic, Antarctic, Tibetan Plateau and Alps. This is especially meaningful for General Circulation Model (GCM) evaluation as ice core records are the only measurements providing BC information from preindustrial to present-day (McConnell, 2010). However, since the number of ice cores is limited, our evaluation includes additional BC observations such as a long-term surface mass concentration and BC in snow measurements from the Arctic regions, which are used to compare with the ACCMIP present-day simulations. Finally, we investigate the BC surface albedo effect with additional modeling. To make it clear, our experiments are not designed to study long-range transport of BC particles. In this paper, we do not include evaluations with remote sensing instruments that are covered in Shindell et al. (2012). Shindell et al. (2012) also include aerosol radiative forcings from the ACCMIP models including BC albedo forcing, but more details of BC albedo forcing are reported in this paper. In Sect. 2, we explain the description of ACCMIP models and simulations used here. Section 3 describes the additional modeling we used to obtain BC albedo forcing and a vertical profile of BC snow concentrations. We present and discuss the model results and BC evaluation using observations in Sect. 4 and BC albedo forcing in Sect. 5. Finally, Sect. 6 is for conclusions.

ACPD
12, 21713–21778, 2012

2 ACCMIP models description

The ACCMIP model descriptions and details information on the ACCMIP projects and simulations are provided in Lamarque et al. (2012a). Here we provide key information about the models and simulations used in this work. Among a total 15 participating models, 9 models include black carbon as a prognostic tracer in their ACCMIP simulations, but only 8 models are used in this paper; LMDzORINCA is excluded in this study due to absence of a required model output. All the models except CICERO-OsloCTM2 are run as coupled chemistry-climate models (CCMs), driven by monthly mean sea-surface temperatures and sea-ice coverage either from observations or from the corresponding coupled ocean-atmosphere model integrations submitted to the Coupled Model Intercomparison Project Phase 5 (CMIP5). The ACCMIP proposed several timeslice runs complementing CMIP5, and the historical runs used in this study consists of 4 core timeslice runs (i.e. 1850, 1930, 1980, and 2000) and 5 tier-1 timeslice runs (i.e. 1890, 1910, 1950, 1970, 1990); GFDL-AM3 and HadGEM2 run 1860 instead of 1850, but these are considered as 1850 for analysis. Model output is not available for all the timeslices. Table 1 summarizes the availability of model BC output for each ACCMIP timeslice run and for the CMIP5 transient historical run. Most models performed the core simulations and only a few models performed the tier-1 simulations. Each timeslice ran for 4 to 10 yr to obtain statistically significant results, except the GISS-E2-R and the CICERO-OsloCTM2. The GISS-E2-R participated with their CMIP5 transient simulations, which covers the entire historical period (1850–2005). The CICERO-OsloCTM2 were run a single year for each ACCMIP timeslice because it is a global chemical transport model (CTM) running with the year 2006 ECMWF (European Centre for Medium-Range Weather Forecasts) reanalysis meteorology for all years. Even with the available ACCMIP timeslice simulations from NCAR-CAM3.5 and MIROC-CHEM, their CMIP5 historical transient simulations were used for BC ice core evaluation as it provides continuous history of model BC deposition from 1850 to 2005.

ACPD
12, 21713–21778, 2012

Table 2 presents brief descriptions of the BC modeling of emission, aging, and deposition. Among 8 models, only 3 models used aerosol microphysics: GISS-E2-R-TOMAS, NCAR-CAM5.1, and HadGEM2. GISS-E2-R-TOMAS (Lee and Adams, 2011) and NCAR-CAM5.1 (Liu et al., 2012) used aerosol microphysics to track aerosol number and mass explicitly based on the sectional scheme and the modal scheme, respectively. HadGEM2 used the modal scheme to track aerosol mass only (Bellouin et al., 2011). For emissions, although the size assumptions are widely varied among models, without aerosol microphysics, this information is unlikely to affect the BC loading. The hydrophilic fraction of emitted BC particles is assumed to be either 0 % or 20 % in models with the exception of HadGEM2 assuming 94.6 % hydrophilic fraction for biomass burning emissions. The larger hydrophilic fraction assumed, the faster BC particles are removed by wet scavenging. All models except NCAR-CAM3.5 inject the biomass burning emissions above the surface layer, and two models inject the BC up to 6 km altitude above the surface. Injection height can play a big role in the lifetime and transport of biomass burning emitted particles (e.g. Sessions et al., 2011). For dry deposition, NCAR-CAM3.5 and CICERO-OsloCTM2 used a constant dry deposition velocity, and the other models used the resistance series method even though the details of the dry deposition parameterization among models vary widely. Wet scavenging of BC particles by ice/mixed-phase clouds can be important in high latitude regions such as the Arctic where most clouds are in ice/mixed-phase. Models account for this scavenging with either 12 % (two GISS models and CICRO-OsloCTM2) or 100 % (GFDL-AM3, HadGEM2 and MIROC-CHEM) of that by liquid clouds. However, NCAR-CAM5.1 does not allow wet scavenging by cloud ice. Most models treated the aging process simply with a fixed e-folding lifetime (i.e. 1–1.6 days). HadGEM2 assumes that BC from fossil fuel emissions remains hydrophobic even when aged and thus only enters cloud droplets through the diffusion scavenging rather than the nucleation scavenging: this accounts for the long lifetime of BC in HadGEM2 (see Sect. 4.1). Although NCAR-CAM5.1 has a microphysical mixing scheme for the aging process that allows the externally mixed BC particles to become internally mixed after coagulation and

ACPD
12, 21713–21778, 2012

condensation with the hydrophilic aerosol components such as sulfate, sea-salt, and organic aerosols, for these simulations the BC was assumed to be internally mixed immediately after emissions. Instead of a fixed value, BC aging lifetime in CICERO-OsloCTM2 depends on season and latitude, based on simulations using the full tropospheric chemistry version of Oslo CTM2 with the M7 aerosol microphysical module (Lund and Berntsen, 2012). The detailed description of each aerosol model is available in the references listed in Table 2: GFDL-AM3 for Donner et al. (2011), GISS-E2-R for Koch et al. (2011), GISS-E2-R-TOMAS for Lee and Adams (2011), NCAR-CAM3.5 for Lamarque et al. (2012b), NCAR-CAM5.1 for Liu et al. (2012), HadGEM2 for Bellouin et al. (2007), CICERO-OsloCTM2 for Skeie et al. (2011), and MIROC-CHEM for Takemura et al. (2000, 2002, 2005).

ACCMIP BC emission

The ACCMIP simulations use the BC emission inventory covering the historical period (1850–2000) provided by Lamarque et al. (2010), which is built for the climate model simulations in CMIP5. The BC emission is largely distinguished by anthropogenic (i.e. originating from energy use in stationary and mobile sources, industrial processes, domestic and agricultural activities) and open biomass burning but is segregated into 12 sectors by a source type listed in Table 3 in Lamarque et al. (2010). Hereafter, anthropogenic BC emissions will be referred to as FF/BF (i.e. fossil fuel and biofuel) emissions, and open biomass burning emissions as BB (i.e. biomass burning) emissions. A few key aspects of the CMIP5 BC emissions are summarized here. This emission inventory is based on previous inventories but has incorporated with new information. The FF/BF emissions are mainly based on Bond et al. (2004, 2007) but applies new emission factors (see Sect. 2.2 in Lamarque et al., 2010, for more details), and the BB emissions are from a combination of three datasets: the GICC inventory for the period of 1900–1950 (Mieville et al., 2010), the RETRO inventory for the period of 1960–1990 (Schultz et al., 2008), and the GFEDv2 inventory for 2000 (van der Werf et al., 2006). This does not provide a vertical profile for BB emissions, and it allows the models to

ACPD
12, 21713–21778, 2012

use different methods to determine an injection height (see Table 2). Finally, emissions are provided every 10 yr, so a linear interpolation is applied for a transient simulation to reproduce interannual variability in a model that might be a poor assumption especially for BB emissions.

Figure 1a shows the total BC emission changes from 1850 to 2000 used in the AC-CMIP historical simulations. All participant models use the same emission rate except the GISS-E2-R that increases BB emission by 40 % to compensate the underestimated BC predictions over the biomass burning regions of Africa and South America (Koch et al., 2009b). The total BC emissions increase almost linearly from 3 Tg (i.e. 1 Tg of FF/BF and 2 Tg of BB) in 1850 to 7.8 Tg (i.e. 5.2 Tg of FF/BF and 2.6 Tg of BB) in 2000 that is mostly due to anthropogenic sources. The emission between 1910 and 1950 is almost constant due to the economic situation and cleaner technology implementation (Bond et al., 2007). BB emissions between 1850 and 1900 are held constant (i.e. 2 Tg per year) (Lamarque et al., 2010).

The BC snow albedo effect is sensitive to the regional changes in BC emissions from preindustrial to present-day as the areas covered with the snow/ice are localized. Thus, we present the spatially distributed FF/BF and BB emissions in 1850, 1930, 1980 and 2000 (see Fig. 1b); the segregated FF/BF and BB emissions by region are presented in Fig. S1 in the Supplement. The historical FF/BF emission evolution is closely related to economic status, air pollution control technology and policy and fuel switch, and the details of this information are available in Bond et al. (2007).

3 The offline land and sea-ice models

Among the 8 ACCMIP models, only 3 models (GISS-E2-R, GISS-E2-R-TOMAS and CICERO-OsloCTM2) calculated BC albedo forcing with their own snow model; in fact, NCAR-CAM5.1 computes the BC albedo forcing, but their albedo forcing is not isolated from other forcing mechanisms. To compute BC albedo forcing and vertically resolved BC snow concentrations, offline land and sea-ice models are used in each

ACPD
12, 21713–21778, 2012

core timeslice (i.e. 1850, 1930, 1980 and 2000) for the 8 ACCMIP models. BC and mineral dust deposition fields from each model were prescribed with monthly resolution (annually-repeating), and linearly-interpolated to the model timestep. All runs were conducted using prescribed meteorology from 1994–2000, with spin-up from 1994–1995 and analysis (averaging) over 1996–2000. The land simulations applied the NCAR Community Land Model 4 (CLM4) (Lawrence et al., 2011), using bias-corrected atmospheric forcing data from Qian et al. (2006), and run at 1.9 × 2.5 degree resolution. The CLM4 has 5 snow layers but the deepest snow layer is not used for the BC snow concentration evaluation: 1st layer (top surface to 2 cm), 2nd layer (2 cm to 7 cm), 3rd layer (7 cm to 18 cm), and 4th layer (deeper than 18 cm). The sea-ice simulations applied the Community Ice CodE 4 (CICE4), using interannually varying atmospheric forcing data from different sources. The CICE4 model has two snow layers: 1st layer (top surface to 2 cm) and 2nd layer (deeper than 2 cm). The land snow treatments of aerosol processes and radiative transfer are described by Flanner et al. (2007) and Lawrence et al. (2011), and the new sea-ice aerosol and radiation treatments are described by Holland et al. (2012). The snow and sea-ice fields generated with these offline configurations agree better with observed conditions during this time period than those simulated with coupled land-ocean-atmosphere simulations, but the precipitation and aerosol deposition fluxes are less compatible with each other than in coupled aerosol-climate simulations. The influence of this incompatibility on simulated surface snow BC concentrations and radiative forcing is somewhat mitigated by the use of temporally-smoothed monthly aerosol deposition fields. Note that greater details of the technique of using offline CLM4 and CICE4 models with prescribed deposition fields will be available in Jiao et al. (2012).

ACPD
12, 21713–21778, 2012

4 Model results and evaluations

4.1 Global-average BC budgets and spatial distributions

In this section, we present the global-average BC budgets and spatial patterns of BC simulations from each model as well as spatial patterns of average and relative standard deviation (RSD) of BC predictions from 8 models, which are referred to as "multi-model mean" (MMM) and "RSD" hereafter. Note that RSD is used to show model diversity and is calculated as a ratio of multi-model standard deviation to MMM. A higher value of RSD represents large model diversity, and zero RSD means no disagreement among models.

Table 3 presents the global-average BC budgets in 1850 and 2000 from each model, MMM and RSD for the corresponding process. Except for GISS-E2-R using 40 % higher BB emissions, all models including GISS-E2-R-TOMAS have the same total BC emissions (i.e. ∼ 3 Tg in 1850 and ∼ 8 Tg in 2000) matching the Lamarque et al. (2010) historical BC emission (see Sect. 2.1; Fig. 1). Global BC burden varies more than a factor of three among the models, ranging from 34 Gg to 103 Gg in 1850 and from 82 Gg to 315 Gg in 2000; excluding HadGEM2, which shows the maximum global BC burden, it reduces to a factor of two variations (i.e. 34–68 Gg in 1850 and 82–169 Gg in 2000). However, the models consistently show that the global BC burden increases by 2.5–3 times from preindustrial to present-day, which is close to the 2.5 times increase in BC emissions occurring in the same period. Global-average BC lifetime is quite varied from 4 days in NCAR-CAM5.1 to 12–15 days in HadGEM2, but these differ insignificantly between 1850 and 2000 for all models except HadGEM2. The long lifetime in HadGEM2 is due to the fact that the BC from FF sources remains hydrophobic even when aged and thus results in slow wet scavenging (Bellouin et al., 2007). Wet deposition is the dominant removal process for BC and its contribution to the total removal rate varies from 53 % in GFDL-AM3 to 95 % in GISS-E2-R-TOMAS; without GFDL-AM3 and GISS-E2-R-TOMAS, it ranges from 74 % to 90 %.

ACPD
12, 21713–21778, 2012

The MMM and RSD of BC budgets in 2000 are compared to Textor et al. (2006) (hereafter, just Textor), which studied model diversity using MMM and RSD of 16 global aerosol models in the framework of the AEROCOM project. It is important to note that the 16 models in Textor did not use consistent aerosol emissions and their BC emission RSD is 0.23 instead of 0.05 in this study. The MMM BC burden in this study is 155 Gg which is about a factor of two less than that in Textor. This discrepancy can be explained by the higher mean BC emissions (~ 12 Tg per year) in Textor. The variation of BC burden among models is slightly lower (RSD = 0.42) in Textor than in the 8 ACCMIP models (RSD = 0.46). For BC lifetime, our MMM is 7.4 days, similar to 7.1 days in Textor, but our RSD is 0.47, which is higher than 0.33 in Textor. The lower model diversity in the Textor BC lifetime likely results from the fact that 12 of the 16 models used the same year reanalysis meteorology, while only one of the ACCMIP models was driven by reanalysis data, so that the higher variation in our BC lifetime (and thus burden) might be caused by variations in the meteorology simulated in each host model and precipitation in particular (Lamarque et al., 2012). This could explain why the diversity in the ACCMIP burdens exceeds the Textor burden diversity even though the ACCMIP simulations uses the same emissions while the Textor BC emission RSD is 0.23. Because all models (except GISS-E2-R) use the same BC emissions, the model diversity of the total deposition flux is negligible. Wet deposition is the dominant removal process for BC aerosols in the ACCMIP models. The MMM of the ratio of wet deposition and total deposition is 0.8 with RSD of 0.16, very close to Textor et al. (2006). Wet deposition rates have small model diversity (RSD = 0.17) but dry deposition rates do not (RSD = 0.63).

The spatial distributions of BC column burden in 2000 for all ACCMIP models are presented in Fig. 2, and the MMM and RSD spatial patterns are shown in Fig. 3a. MMM and RSD spatial patterns are computed after re-gridding the model outputs into 2° in latitude and 2.5° in longitude. In general, the model BC burden distributions show a large model diversity that tends to increase away from the source areas due to the large influence of the aerosol transport and deposition processes on the burden. The

ACPD
12, 21713–21778, 2012

NH high latitude regions and some remote regions show RSD of 0.8 or higher, which means the standard deviation is as large as (or more than) the mean. On the other hand, the high emission regions tend to have RSD of less than 0.3.

The MMM and RSD distributions of the total BC deposition fluxes are shown in Fig. 3b using a global map and Fig. 3c using the Arctic-centered map to provide a better look over the Arctic. In general, the spatial patterns of MMM are roughly similar to the emissions shown in Fig. 1b and the column burden distribution in Fig. 2. Unlike the large diversity in the column burden distribution in Fig. 3a, the BC deposition fluxes display much smaller model diversity than the column burden. This is consistent with what we saw in the global-average budgets. Model deposition fluxes diverge significantly over the Southern Hemisphere (SH) high latitude. Figure 3c displays the relatively large model diversity over the Arctic regions especially near Greenland. Interestingly, although the RSD distributions of column burden and deposition fluxes show an increasing RSD away from the source regions, the lowest RSD in the deposition fluxes distribution seems to be over BB emission regions while the lowest RSD in the column burden distribution seems to be over FF/BF emission regions. This feature is not related to the 40 % enhanced BB emissions in GISS-E2-R as this was reproduced without GISS-E2-R (not shown). This might be related to the BB injection height, but we did not investigate this further.

To display the spread among 8 ACCMIP models for the spatial distributions of modeled BC between 1850 and 2000, MMM and RSD is computed based on a ratio of BC column burden in 2000 to that in 1850 from each model (shown in Fig. 4). In the same manner, the MMM and RSD of the deposition flux changes in 2000, 1980, and 1930 relative to 1850 are computed and are presented in Fig. 5. The changes in the column burden and deposition fluxes are quite similar, displaying overall increases over the globe and some decreases over small parts of US and Europe due to FF/BF emission and some parts of South America and Australia due to BB emissions. The RSD of the BC changes between 2000 and 1850 are mostly lower than 0.3–0.4 except in high latitude regions. Compared to Fig. 3a, Fig. 4 shows relatively small model diversity

ACPD
12, 21713–21778, 2012

because each model's removal parameterizations behave similarly in 2000 and 1850. Over SH high latitude areas, we observed high model variations in the deposition flux (in Fig. 3b) in 2000 and also in the deposition flux changes in 2000 and 1980 relative to 1850 (in Fig. 5). Compared to the SH mid-latitude, the SH high latitudes exhibit a higher increase in BC deposition fluxes starting from 1980. Given that the SH high latitude regions are far from the source regions, this suggests increasing BC transport into this region. Thus, the larger model diversity might be due to the substantial diversity in aerosol transport among models, which is especially significant in the 1980 and 2000 simulations with increasing BC emissions in SH subtropics. In Fig. 5, the changes in 1980 relative to 1850 are quite similar to 2000 except for the higher increase observed over Europe in 1980 due to the emission. The BC deposition fluxes increase noticeably from 1850 to 1930 over Western Europe and North American where there is a large FF/BF emissions increase due to the economic growth, while the deposition decreases over the high latitudes of South America and North America due to reduced BB emissions.

4.2 Surface BC mass concentrations and CO mixing ratios

To evaluate the ACCMIP 2000 BC predictions, we used the long-term surface BC mass concentrations obtained from the National Oceanic and Atmospheric Administration Earth System Research Laboratory Global Monitoring division (NOAA-ESRL-GMD, http://www.esrl.noaa.gov/gmd/), the European Monitoring and Evaluation Program (EMEP) network (via the EBAS website hosted at Norwegian Institute for Air Research, http://ebas.nilu.no), and the Atmospheric Radiation Measurement (ARM) in Department of Energy (http://www.arm.gov) – Jungfraujoch (as part of EMEP network), Alert and Pallas BC data were obtained separately. Table 4 lists the 14 observation sites for BC surface mass concentrations used in this study including the site coordinates, site category, measurement time periods, and the details of the measurements. Note that, hereafter, Ny-Ålesund and Hyytiälä are simply written as Ny-Alesund and Hyytiala, respectively. Also note that the EMEP network BC data as well as the

ACPD
12, 21713–21778, 2012

BC in Alert and Pallas were provided as a mass concentration whereas the BC data from the NOAA-ESRL-GMD were an absorption coefficient and thus were converted into a mass concentration by assuming a mass absorption cross section of 9.7 $m^2 g^{-1}$, following Skeie et al. (2011). When BC data were provided at multiple wavelengths including 880 nm from Aethalometer, which is the case for most EMEP data, we chose to use BC concentrations at the 880 nm wavelength channel because the BC mass concentration measured at this wavelength is considered to represent the BC in the atmosphere: at this wavelength BC is the principal absorber of light and other known aerosol components have negligible absorption. Within the information we were able to collect, the Prelia BC data at 880 nm from the Aethalometer was converted with a mass absorption cross section of 16.6 $m^2 g^{-1}$, a default value set by the manufacturer for a wavelength of 880 nm, (Vidmantas Ulevicius, personal communication, 2012). The Ny-Alesund data were treated with 15.9 $m^2 g^{-1}$ (Eleftheriadis et al., 2009), and for the Mace Head data, 19 $m^2 g^{-1}$ before May 2005 and 16.6 $m^2 g^{-1}$ after May 2005 (Junker et al., 2006; Gerard Jennings, personal communication, 2012). The Jungfraujoch BC data (Collaud Coen et al., 2007) was prepared using the method described in Collaud Coen et al. (2010). The BC data in Alert were converted using 19 $m^2 g^{-1}$ from October to May and 28 $m^2 g^{-1}$ from June to September to match with EC measurements (Sharma et al., 2002; S. Sharma, personal communication, 2012), and BC in Pallas (Hyvarinen et al., 2011) used the conversion method followed by Weingartner et al. (2003). Barrow data included only values from the clean air sector in order to avoid local contamination by emissions from the town of Barrow, and Mauna Loa data only included nighttime data to minimize exposure to local pollution sources (Bodhaine, 1995; Betsy Andrews, personal communication, 2012). Some of the BC measurement stations listed in Table 4 also provide a long-term measurement of carbon monoxide (CO) mixing ratio, so the modeled CO seasonality is also evaluated to the monthly mean of the measured CO mixing ratios that was averaged with available data between 1996 and 2005. Since CO tracer has a long lifetime ($\sim$ 2 month), we used the seasonality of CO mixing ratio as a rough proxy to diagnose BC aerosol transport issue.

ACPD
12, 21713–21778, 2012

Figure 7 shows the seasonality of BC mass concentrations in the model surface layer compared to the measurements listed in Table 4. We provide the statistical measures at each station for each model including correlation coefficient (R), log-mean normalized bias (LMNB) and log-mean normalized error (LMNE) in Table S1 in the Supplement. The measured BC concentrations in the Arctic stations (i.e. Alert, Barrow and Ny-Alesund) exhibit a similar magnitude and seasonality with the minimum during the late summer and the maximum during the late winter and early spring. This seasonality pattern can be explained with the seasonal variations of transport pathways and deposition processes especially wet deposition that is a result of atmospheric circulation in the Arctic known as the polar dome (e.g. Stohl, 2006; Law and Stohl, 2007; Quinn et al., 2007). During winter, the polar dome typically extends toward more southerly latitudes than in summer, allowing low-altitude transport poleward (i.e. faster transport compared to the high-altitude transport) and limiting deposition processes as the Arctic is stable and dry (Law and Stohl, 2007). In contrast, the summer polar dome eliminates direct low-level transport from the surrounding continents and enhances wet scavenging by forming frequent drizzle (Stohl, 2006). Garrett et al. (2011) use long-term surface CO and BC measurements to show that enhanced wet scavenging during summer is a more important driver for the Arctic BC seasonality than inhibited transport. At three Arctic stations, HadGEM2 captures the observed seasonality quite well (i.e. over R of 0.7 and LMNB of 0.4–0.6) but overestimates BC mass concentrations significantly in summer and fall. The two GISS models are able to capture the seasonal cycle at Alert and Ny-Alesund with R of $\sim$0.8, but their prediction at Alert is poor especially during winter and spring seasons. Overall, the BC predictions vary by more than two orders of magnitude among models, and most models underestimate the BC concentrations severely in winter and spring with a difficulty to capture the seasonality. Unlike BC, the CO seasonality is very similar among three stations and is fairly good even with some underpredictions during the late winter and early spring (see Fig. 8). Also, the model diversity is very small. This may suggest that scavenging rather than transport is a primary cause for the poor BC seasonality and the large model diversity. In fact, the poor

ACPD
12, 21713–21778, 2012

seasonality of BC mass concentrations at these Arctic stations has been also shown in previous studies (Shindell et al., 2008; Huang et al., 2010b; Liu et al., 2011; Skeie et al., 2011; Browse et al., 2012; Wang et al., 2012). Several model studies (Huang et al., 2010b; Liu et al., 2011; Wang et al., 2011a, 2012; Browse et al., 2012) showed that the large underprediction of the Arctic BC could be improved by adjusting the treatment of wet scavenging: Liu et al. (2012) used GFDL-AM3 and Wang et al. (2012) used CAM5.1, but the modified scavenging schemes were not applied to their ACCMIP simulations. However, it is important to mention that the deviation in the Arctic BC mass concentrations among the ACCMIP models cannot be explained by the difference in a single process such as the ice/mixed clouds wet scavenging scheme or the BC aging (see Table 2). Unfortunately, none of these studies investigated the impact of the modification of wet scavenging on BC deposition over snow and ice surfaces in the Arctic.

The modeled BC concentrations at European stations (i.e. Pallas located in the sub-Arctic region, Hyytiala, Mace Head, Preila, Jungfraujoch and Ispra) show much less model diversity than in the Arctic stations and capture the measured BC mass concentrations mostly within factor of 2 of the observation (i.e. LMNE < 0.3) except at Jungfraujoch and Ispra. However, the seasonal cycles are widely different among models, as this is also reflected with the wide range of R values. The measured BC seasonality at high-latitude European stations (Pallas, Hyytiala, Mace Head, and Prelia) resembles the Arctic seasonality especially sustaining a higher concentration during the late winter to early spring, although most models cannot capture this. The CO seasonality at those sites also looks close to the Arctic with very small variation among models. At Jungfraujoch, the model BC is significantly overestimated but their seasonal cycle are actually captured well in 5 models with R of over 0.8.

At most North American stations (i.e. Sable Island, Bondville, Southern Great Plains and Mauna Loa), in general, the model BC concentrations agree within a factor of 2 of the observations. In general, they show a very weak seasonality. Similarly, the CO seasonality is quite weak at Southern Great Plains. However, Trinidad Head and

ACPD
12, 21713–21778, 2012

Mauna Loa have a distinctive seasonality of CO. At Trinidad Head, most models did not capture the observed seasonality properly as the models peak 1–2 months earlier. This same behavior is also captured in the CO plot in Fig. 8.

4.3 Present-day BC snow concentrations in the Arctic

Recent measurements of BC snow concentrations (Hegg et al., 2009, 2010; Doherty et al., 2010) were performed in Alaska, Canada, Greenland, Svalbard, Norway, Russian and the Arctic Ocean mostly in spring by sampling the full snowpack depth (mostly down to the top few to tens of centimeters). These measurements can provide information on the BC deposition during the corresponding snow season. We obtained the measurement data from http://www.atmos.washington.edu/sootinsnow/ArcticSnowBC.php. Since BC snow concentrations were not available directly from the ACCMIP models, we performed the additional set of simulations using the offline land and sea-ice models running with prescribed meteorology and aerosol deposition fields from each ACCMIP model (see Sect. 3 for more details). It is important to keep in mind that the ACCMIP simulations did not apply interannually-varying emissions and simulated deposition fields are more consistent with each model's meteorology than that used to force the offline land and sea-ice simulations. To obtain a vertical profile of BC snow concentrations, the offline land model used a sophisticated BC-snow model developed by Flanner et al. (2007). For this work, we used the same "inefficient" melt scavenging parameters applied by Flanner et al. (2007), meaning that aerosols accumulate at the surface during snow melting. Limited field observations also show melt-induced impurity accumulation at the snow surface (Conway et al., 1996; Xu et al., 2012). To compare the observed data and the modeled BC, we first prepared the observation and the model data in the following way; (1) the observed data are averaged when falling into in the same model gridcell and snow layer; (2) the modeled data are averaged over 5 yr simulations (1996–2000) and sampled for the month of observations. The observation year was not a critical sampling condition in our case, and we provide the reasons later.

ACPD
12, 21713–21778, 2012

Figure 9 shows the scatter plots of the modeled BC snow concentration (ng of BC per g of snow) and the observed values in 8 regions consistent with the regional classification used in the original observation data: Arctic Ocean, Canada sub-Arctic, Canadian Arctic, Alaska N. Slope, Ny-Alesund, Tromsø (hereafter, just Tromso), Greenland and Russia. The LMNB and LMNE are computed for each region and each model (see Table S2 in the Supplement). Based on the LMNB and LMNE values, the modeled BC concentrations are, on average, within a factor of 2–3 of observed BC and observations, except for in the Arctic Ocean and Greenland,. Models overpredict Greenland BC, on average, by a factor of 4 to 8. For the Arctic Ocean, modeled BC is underpredicted, on average, by a factor of 2–5 (but 22 times for NCAR-CAM5.1). Compared to previous modeling studies (Skeie et al., 2011; Wang et al., 2011a), our model to observation agreements seem to be poorer. This is likely because the CMIP5 emission is decadal-scale, which is especially inappropriate for BB emissions. In fact, the observations report a significant contribution of BB emissions to the Arctic BC snow concentrations (Hegg et al., 2009, 2010). Also, Wang et al. (2011a) attribute 60 % of the Arctic BC in snow in spring 2008 (40 % in springs 2007–2009) to BB emissions based on GEOS-CHEM simulations.

Regarding the sampling method, the observation year was less critical in this study because (a) the ACCMIP simulations do not account for interannual variations in emissions, (b) the prescribed meteorology from 1996–2000 used in the offline models does not cover much of the observation periods (1998 and 2005–2009), and (c) the model results are quite insensitive to sampling with/without the observation year, based on the additional simulations we conducted with prescribed meteorology from 2000–2008. In fact, we initially ran the offline land and sea-ice models using reanalysis meteorology from 2000 to 2008 with deposition field from 4 ACCMIP models (GFDL, GISS-E2-R, CICERO-OsloCTM2, and MIROC-CHEM). Using the 2000–2008 meteorology, we found little difference in model results between when sampled for the year of observations and averaged from 2000 to 2008. Model BC snow concentrations decreased somewhat when using 1996–2000 meteorology compared with 2000–2008, especially

ACPD
12, 21713–21778, 2012

over Russia and the Arctic Ocean. This did not change the model to observation agreements much, however, in any region except the Arctic Ocean. For Russia, although the BC snow concentrations were reduced enough to change from overprediction to underprediction, for both cases models agree with the observations, on average, within a factor of two (not shown). Even though some of the Arctic Ocean data were actually sampled in 1998, models agree with the observations much better using the 2000–2008 meteorology (i.e. overpredict BC within a factor 2–3 of the observation vs. underpredict within a factor of 2–5 for 1996–2000 meteorology). This suggests that the Arctic BC snow concentrations are not insensitive to the choice of the meteorology period applied, especially over the Arctic Ocean and Russia, or to interannual variations in BC emissions.

4.4 Historical BC ice-core concentration (1850–2000) evaluations

Aerosols in GCMs are mostly evaluated with observations from recent years to recent decades. Ice core records, possibly the only datasets to provide long-term historical information on aerosols, are definitely extremely valuable for GCM model evaluations (McConnell, 2010) even with only a few datasets available. Ice core evaluations in previous studies have been done either using BC deposition fluxes (Lamarque et al., 2010) or BC snow concentrations (Koch et al., 2011; Skeie et al., 2011); Koch et al. (2011) adjusted the modeled BC snow concentrations with the ice core precipitation data. In this study, we use BC snow concentrations, BC deposition fluxes, and precipitation, despite their close relationships. This is because BC snow concentrations are most relevant for BC albedo forcing, while BC deposition fluxes and precipitation are directly simulated in a model and therefore their evaluation is very useful for models. Note that we do not examine matching between the model topography and the altitude of the ice core site since this information was not available for all models. It might be questionable how well a GCM model performs over the Arctic, the Antarctic, and the high mountain glacier regions especially with a coarser grid resolution, but this topic is beyond the scope of our work. It is also important to mention that our discussions on the model

ACPD
12, 21713–21778, 2012

temporal trends are quite limited to the emission patterns because our simulations do not track BC emitted from various source regions separately.

Table 5 presents 12 BC ice core sites used to evaluate the historical BC predictions from the ACCMIP models: 4 sites in Greenland, 5 sites in the Tibetan Plateau, 1 site in the Alps (i.e. Colle Gnifetti glacier) and 2 sites in Antarctica; additionally, we included BC ice core from the Fiescherhorn glacier in the Alps (Jenk et al., 2006), which is presented separately in the Supplement. We present the evaluation of modeled BC deposition fluxes (Fig. 10), BC snow concentrations (Fig. 11) and annual precipitation (Fig. 12) using the ice core data. Note that the same figure as Fig. 11 but with smaller Y-axis scale is shown in Fig. S2 in the Supplement to display the observed BC concentrations more clearly. A few notes here: (1) The Alps data are only used for BC snow concentrations due to the absence of precipitation data (and thus missing BC deposition fluxes). Specifically, the accumulated precipitation is impossible to obtain at this site because of the removal of winter snow by wind (Florian Thevenon, personal communication, 2012). (2) For BC deposition fluxes evaluations, we used the CMIP5 transient simulations for NCAR-CAM3.5 and MIROC-CHEM instead of their equivalent timeslice simulations. (3) Modeled BC snow concentrations are computed using total BC deposition fluxes and precipitation rate, assuming all precipitation falls as snow, which is an a reasonable assumption at these ice core sites. (4) Ice core observation data in Figs. 10 to 12 are presented as 5-yr running averages (thick black lines) along with annual-average (black dots) to reduce interannual variations. This helps to make it more comparable to our simulations, which are based on climatological-meteorology and decadal-scale BC emissions. BC emissions in the CMIP5 transient simulations are interpolated linearly between two adjacent decades and therefore might not represent a realistic interannual variation.

For the Antarctic stations, WAIS and Law Dome (Bisiaux et al., 2012a; Bisiaux et al., 2012b) show the lowest BC deposition fluxes (and BC snow concentrations) among sites and little change throughout the period. For example, comparing the average from 1850 to 1859 to that from 1996 to 2001–2002 for the ice core observation, the WAIS ice

ACPD
12, 21713–21778, 2012

core records increase from 0.08 to 0.12 ng g^{-1} for BC snow concentrations and from 15 to 21 μg m^{-2} yr^{-1} for BC deposition fluxes; for Law Dome, no changes for BC snow concentrations and from 26 to 34 μg m^{-2} yr^{-1}. Although Bisiaux et al. (2012b) relate the BC ice core temporal trend to ENSO variability, we cannot investigate any linkage with the ENSO event because our simulations are based on the decadal average SSTs. The model diversity of BC deposition is very large at the Antarctic sites as shown in Figs. 3 and 4b. NCAR-CAM3.5, MIROC-CHEM, GFDL and NCAR-CAM5.1 agree better with the observations, but MIROC-CHEM overpredicts the relative changes between preindustrial to present-day in both Antarctic stations significantly because of the underprediction in the preindustrial period. For GISS-E2-R, GISS-E2-R-TOMAS, HadGEM2 and CICERO-OsloCTM2, their relative changes between preindustrial to present-day are similar to the observation even with their overpredictions. Model overpredictions of BC snow concentrations at Law Dome are less than for BC deposition fluxes because of overprediction of precipitation (see Fig. 12). Figure 4 in Bisiaux et al. (2012b) shows similar decreasing trends during the 1950s to the 1980s between the observed BC and SH grass fire emissions that are used in this study. However, the three ACCMIP models with the CMIP5 transient simulations exhibit increasing BC concentrations during the same period, which seems to resemble the overall SH emissions (or the SH fossil fuel and forest fire emissions) trend rather than grass fire emissions.

The five Tibetan Plateau (TP) ice cores (Xu et al., 2009a) are widely spaced on the TP (Fig. 6a) and extend back to the 1950s. The BC deposited in the TP glaciers shows higher BC deposition/concentrations than other regions because of the proximity to the large BC emission areas. They have strong seasonality (i.e. high in winter and low in summer) that can be characterized by a dominant westerly jet stream and dry weather conditions in winter and the South Asian Monsoon and wet weather conditions in summer (Ming et al., 2008; Xu et al., 2009a; Wang et al., 2011b). The westerly jet stream brings BC mostly from Europe, the Middle East, the Former USSR and North Africa while the summer monsoon brings BC from the south and southwestern areas including South Asia (Lu et al., 2012). The westerly jet stream plays an important role

ACPD
12, 21713–21778, 2012

in transporting BC aerosols all year in the northern and northwestern TP regions (i.e. Muztagh Ata and Taggula).

Regarding BC temporal trends, as shown in Figs. 10 and 11, the TP BC ice core records display strong temporal variations from the 1950s to the 2000s that are not captured in the models. Xu et al. (2009) pointed out that all TP ice core records except Zuoqiupu show the declining BC concentration during the 1950s–1960s possibly due to the decreasing European emissions. Instead of decreasing, the modeled BC increases steadily since the 1950s except MIROC-CHEM, which shows a very slight declining trend between the 1930s–1940s and the 1960–1970s. For the BC emissions used in this study, we found that the Western European emissions decrease during that period but the Eastern European emissions increase, which is similar to the model BC deposition history (Fig. S1); the total BC emissions in Western and Eastern Europe fluctuate a little but do not clearly decrease during that period. This might indicate that, even though the Eastern Europe is located closer to the TP, BC deposition in the TP ice cores is more influenced by the Western Europe. In Muztagh Ata, which is most likely influenced by the westerlies all year, the modeled BC in the 1980s is higher than that in the 2000s, which is also consistent with the Eastern European emission trend because the Western European emissions keep decreasing. At Zuoqiupu, the BC ice core shows an increasing trend from the 1980s without the high BC concentrations in the 1950s–1960s, possibly because of the unfavorable transport path from the European emissions to that site (Xu et al., 2009a). The temporal trend at Zuoqiupu is well captured by the models. In contrast to the temporal trend in the BC ice core record at Rongbuk from Ming et al. (2008) (i.e. shown the red line in Fig. 11), the BC ice core record from Mt. Everest spanning 1860–2000 (Kaspari et al., 2011), which matches the same location of Rongbuk glaciers used here, does not exhibit the high BC concentration in the 1950s–1960s but shows a similar trend as Zuoqiupu. However, this should be viewed cautiously because the BC ice core records in Kaspari et al. (2011) are unusually low (below 1 ng g^{-1}, close to the Antarctic BC ice cores).

ACPD
12, 21713–21778, 2012

Despite missing the strong temporal variations of BC in the TP areas, the time mean of the modeled BC depositions at Muztagh Ata, Tanggula and Noijin Kangsang are consistent with the observed values, with GISS-E2-R, GISS-E2-R-TOMAS and NCAR-CAM5.1 showing excellent agreement (see Fig. 10). All models underpredict the BC deposition significantly at Rongbuk and Zuoqiupu. Compared to the BC deposition fluxes, BC concentrations by GISS-E2-R and GISS-E2-R-TOMAS agree slightly worse at Muztagh Ata while the model overprediction is much reduced at Rongbuk (see Fig. 11). These changes are explained by the precipitation biases (see Fig. 12).

We also evaluate the simulated BC concentrations and precipitation during the monsoon season (June to September) and non-monsoon season (October to May) at Zuoqiupu (Fig. 13). Note that we present the same plot as Fig. 13 but with smaller Y-axis scale in Fig. S3 in the Supplement to show the observed BC concentrations better. The observed BC concentration in Fig. 13 was treated with a 5-yr running average. The observed precipitation data are simply derived using a 5-yr running average of BC concentrations separated into the two seasons, annual BC concentrations and annually accumulated precipitation. Although the BC concentrations are underpredicted regardless of season, most models predict BC concentrations that are 2–4 times higher during the non-monsoon season than monsoon season, which is consistent with observations. Precipitation at Zuoqiupu is captured well by the models.

Greenland ice core records at D4 (McConnell et al., 2007), ACT2 (McConnell and Edwards, 2008), Summit and Humboldt (McConnell, 2010) are most frequently used in previous studies (Lamarque et al., 2010; Koch et al., 2011; Skeie et al., 2011). Both models and observations exhibit a large interannual variation in Greenland (Figs. 10 and 11). All Greenland ice cores show a peak in the 1910s–1930s that is consistent with the highest BC emissions in the North America and Western Europe in the same period. This signature is also captured very well in the models. Interestingly, the models simulate an increasing trend after the 1960s–1970s using BC deposition fluxes, but this trend does not appear in the BC concentrations or in the ice core records. For BC deposition fluxes, all models except NCAR-CAM5.1 capture the observation quite well

ACPD
12, 21713–21778, 2012

(within a factor of two) until approximately the 1960s. The underprediction of BC surface mass concentration and overprediction of BC deposition fluxes in the 2000s suggests a problem with deposition. For BC concentrations, our models agree relatively well with the observations except at Summit. However, model to observation agreement for BC concentrations is not as good as that for deposition fluxes due to the biases in the simulated precipitation.

Similar to the Greenland ice cores, modeled BC at the Alps peaks in the 1930s, reflecting the influence of neighboring European emissions. From 1850 to 1950, the Alps ice core, from the Colle Gnifetti glacier, (Thevenon et al., 2009) shows no clear increase because of particularly high concentrations from the 1850s to the 1890s (e.g. 12 ng g^{-1} for the 1890–1948 average, 14 ng g^{-1} for the 1850–1889 average or 11 ng g^{-1} for the 1850–1889 average excluding years with over 20 ng g^{-1}). However, when including the observed BC from 1750 and excluding the high BC concentrations during the 1850–1890 periods, the Alps BC concentrations increase over time (e.g. 9 ng g^{-1} for the 1750–1889 average). The high concentrations during the 1850s–the 1890s do not appear in the BC ice core from the same glacier in the Alps in Lavanchy et al. (1999), but the two BC records have quite different BC concentrations. These differences might result from the different measurement techniques applied to determine BC particles. Nevertheless, both Alps BC ice cores consistently show BC increasing by 2–3 times from the 1750–1890 period to the 1950–1975 period due to the regional emission changes (Lavanchy et al., 1999; Thevenon et al., 2009). Gabrieli et al. (2010) find organic pollutants deposited in the Colle Gnifetti glacier, the same ice core as Thevenon et al. (2009), are influenced by neighboring European emissions. This agrees with the increase in the modeled BC concentrations, although the models seem to show the higher concentration in the 1930s, which agrees with the emissions changes in the ACCMIP models. We obtained the additional data from the Alps EC ice core extracted from the Fiescherhorn glacier (46.55° N, 8.07° E, 3900 m), which are available from Table S2 in Jenk et al. (2006), and we find that our models agree quite well (see Fig. S4 under the Supplement). Overall, our models and three Alps BC/EC ice cores suggest

ACPD
12, 21713–21778, 2012

that the BC particles deposited in the Alps are most influenced by the neighboring European emissions.

5 BC albedo forcing

Global annual average BC surface albedo forcing is computed using the NCAR CLM4 and CICE4 models with the offline methodology described in Sect. 3. Results are presented in Fig. 14a for 1930, 1980, and 2000 relative to 1850 (hereafter, referred to as "offline" BC albedo forcing). The highest global annual average BC albedo forcing occurs in 1980, and the forcing in 1930 is similar to 2000. Our offline BC albedo forcing in 2000 ranges from 0.014 $W m^{-2}$ to 0.019 $W m^{-2}$ among the ACCMIP models, which differ little among models: 40 % difference for the 2000 forcing, 54 % for the 1980 and 68 % for the 1930. This is likely due to our method of using the same offline model and meteorological data (producing identical snow cover) to compute the albedo forcings for all deposition fields. Flanner et al. (2007), who applied the same snow albedo model with a coupled atmosphere-land-ocean configuration (CAM3), report a total BC albedo forcing of 0.05 $W m^{-2}$ (relative to no BC), larger than the ACCMIP range of year 2000 total BC albedo forcings found here (0.024–0.037 $W m^{-2}$: relative to no BC instead of 1850). These differences arise partly because the offline methodology, applied here, produces less snow cover over the Tibetan Plateau and other parts of Asia that were subject to large forcing in the Flanner et al. (2007) study, leading to smaller forcing (see Fig. 15). Also, because the forcings for all time periods were quantified using snow and ice states representing the 1996–2000 period, which are likely diminished relative to previous periods, actual BC snow forcing in 1850 may have been greater (Lawrence et al., 2012).

Three ACCMIP models including CICERO-OsloCTM2 and two GISS models compute the albedo forcing in their host model (hereafter, referred to as "online" BC albedo forcing). We compare global annual average online BC albedo forcing with the offline BC albedo forcing in Fig. 14b. They agree well on temporal pattern with the highest

ACPD
12, 21713–21778, 2012

forcing in 1980. Interestingly, even with the same parameterization of BC albedo effect used for GISS-E2-R and GISS-E2-R-TOMAS, the online BC albedo forcing is a factor of two lower than the offline forcing for GISS-E2-R and, for GISS-E2-R-TOMAS, 20 % higher. It seems that the parameterization used in the GISS models (Koch et al., 2009a) is much more sensitive to the BC deposition fluxes. Like GISS-E2-R, the CICERO-OsloCTM2 offline BC albedo forcing is also 2 times higher than the estimates from their own model. This suggests that BC-snow parameterizations and model snow cover can strongly influence forcing (Flanner et al., 2007). It is worth mentioning that CICERO-OsloCTM2 shows little change in the present-day BC albedo forcing when switching from the Bond et al. (2007) anthropogenic BC emission dataset to the Lamarque et al. (2010) dataset: Skeie et al., (2011) reports BC albedo forcing of 0.008 $W m^{-2}$ based on 2006 meteorology only due to the anthropogenic emissions changes (i.e. FF/BF) based on Bond et al. (2007). However, the time evolution of global annual BC albedo forcing in Skeie et al. (2011) is slightly different as a higher forcing is found in 1930 than in 1980. This shows that BC albedo forcing is sensitive to the changes in regional BC emissions, which might slightly differ between Lamarque et al. (2010) and Bond et al. (2007), though the BC emissions in Lamarque et al. (2010) are heavily based on Bond et al. (2007). Bauer and Menon (2012) estimate global annual mean BC albedo forcing of 0.016 $W m^{-2}$, based on the MATRIX aerosol microphysics model (Bauer et al., 2008) in the same GISS GCM model as GISS-E2-R and GISS-E2-R-TOMAS, and using the same emissions (Lamarque et al., 2010). The main difference among these models is their aerosol representation. The estimate from Bauer and Menon (2012) falls in between 0.009 $W m^{-2}$ (GISS-E-2-R) and 0.022 $W m^{-2}$ (GISS-E2-R-TOMAS). Based on the GISS models, we find that differences in aerosol representations within the same GCM can produce more than a factor of two difference in global annual mean BC albedo forcing.

Figure 15 shows the spatial patterns of BC albedo forcing in 2000 and 1980 relative to 1850. In 2000, BC albedo forcing is positive everywhere with the highest BC forcing (i.e. over 0.2 $W m^{-2}$) over Manchuria and Karakoram areas and relatively high forcing

ACPD
12, 21713–21778, 2012

(i.e. over 0.1 $W m^{-2}$) over most of the Former USSR. Most Arctic areas show small positive forcing. In 1980, the highest BC forcing (i.e. over 0.8 $W m^{-2}$) is seen over a large area in the Former USSR. This is due to the high FF/BF emissions in the Former USSR in 1980 compared to 2000 (see Fig. S5 in the Supplement). The BC albedo forcing estimates diverge the most over Greenland, North America and the Tibetan Plateau for both the 2000 and 1980 cases (not shown).

6 Summary and conclusions

The main goal of the Atmospheric Chemistry and Climate Model Intercomparison Project (ACCMIP) is to investigate the influence of atmospheric gases and aerosols on climate change (Lamarque et al., 2012a). As part of the ACCMIP, this work aims to evaluate preindustrial to present-day black carbon (BC) aerosols in the 8 ACCMIP models against 12 ice core records from Greenland, Tibetan Plateau, Alps, and Antarctica. Among 15 ACCMIP models, 8 models tracking BC aerosols as a prognostic tracer are used: GFDL-AM3, GISS-E2-R, GISS-E2-R-TOMAS, NCAR-CAM3.5, NCAR-CAM5.1, HadGEM2, CICERO-OsloCTM2 and MIROC-CHEM. We also evaluate the present-day BC predictions with long-term atmospheric BC surface mass concentrations and recent BC snowpack measurements from the Arctic regions. With the monthly mean deposition fields of BC and mineral dust from each model, we estimate BC albedo forcing with additional simulations using the NCAR CLM4 and CICE4 models, which include sophisticated BC-snow and BC-ice treatments (Flanner et al., 2007; Lawrence et al., 2011; Holland et al., 2012). To evaluate with recent snowpack measurements, we obtained a vertical profile of BC snow concentrations from the additional simulations.

The ACCMIP historical simulations were performed as timeslice experiments; core (i.e. essential) simulations include 1850 (i.e. preindustrial), 1930, 1980, and 2000 (i.e. present-day) timeslices, which all models participated in, and tier 1 (i.e. useful) simulations includes 1890, 1910, 1950, 1970, and 1990 timeslices, which only a few models did (see Table 1). All simulations were based on the anthropogenic and biomass

ACPD
12, 21713–21778, 2012

burning emissions inventory created for the Climate Model Intercomparison Project phase (CMIP5) (Lamarque et al., 2010). For the ice core evaluation, the CMIP5 historical transient simulations were used for NCAR-CAM3.5 and MIROC-CHEM: GISS-E2-R participated in the ACCMIP with their CMIP5 transient simulations.

We first examined the global annual budgets of BC emission, deposition, and lifetime in 1850 and 2000 from each model. Global annual BC emission rate is increased from $\sim 3\,\mathrm{Tg\,yr^{-1}}$ to $\sim 8\,\mathrm{Tg\,yr^{-1}}$, mostly driven by anthropogenic emissions. Global BC burden differs approximately a factor of 3 among models: 34 Gg to 103 Gg in 1850 and 82 Gg to 315 Gg in 2000. Similarly, BC lifetime varies from 4 days to 15 days with a negligible change between 1850 and 2000. This large model diversity stems from the differences in aerosol removal parameterizations and also from simulated meteorology among models. The dominant removal process for BC in models is wet deposition, contributing 80 % of the total deposition rate on average among models. For the relative changes between two timeslices (e.g. 1850 vs. 2000), models agree quite well because of the similar behavior in each model's own parameterizations for aerosol removals between two timeslices. For instance, the global BC burden from preindustrial to present-day increases by $2.5 \sim 3$ times, which is close to the 2.5 times increase in BC emissions, suggesting that emissions are a main driver for the BC burden changes. Comparing spatial distributions of BC burden in the present-day simulations from each model, we notice that models diverge the most at both NH and SH high latitude regions. However, only SH high latitude regions appear to be noticeably divergent for BC deposition fluxes. Compared to 1850 simulations, models show increasing BC deposition over the Antarctic regions in 1980 and 2000 with particularly larger model diversity. This suggests significant model diversity in aerosol transport, which becomes important with increasing BC transport into the Antarctic. This model behavior is also found in the ice core evaluation.

For BC in the present-day ACCMIP simulations, we find that the simulated Arctic atmospheric BC surface mass concentrations are severely underestimated during the winter and spring, leading to a poor seasonality. Based on our CO evaluations and

ACPD
12, 21713–21778, 2012

previous studies (Huang et al., 2010b; Liu et al., 2011; Browse et al., 2012; Wang et al., 2012), the wet scavenging scheme seems to be one of key processes to improve the Arctic BC seasonality in models. In general, the models capture the observed BC mass concentrations well in Europe and North America except at Jungfraujoch and Ispra. With the recent snowpack measurements, we find that the model's vertically resolved BC snow concentrations are, on average, within a factor of 2–3 of the measurements except for Greenland and the Arctic Ocean. Missing interannual variations in our emission dataset seem to contribute a considerable scatter in model to observation agreements compared to previous studies. During this evaluation, we found that the choice of meteorological period used to simulate the BC snow concentrations in the offline land and sea-ice models has a moderate impact on BC snow concentration and is larger over the Arctic Ocean and Russia.

For preindustrial to present-day BC in the ACCMIP models evaluated with the ice core records, some models overpredict BC deposition fluxes/ice-core concentrations in the Antarctic sites, and some models capture the observed magnitude quite well throughout the period. Modeled BC deposition fluxes increase during the 1950s to the 1980s, which might be due to rising SH total BC emissions, while the ice core records are correlated better with the declining SH BB emission during this period. However, models are able to capture the relative changes from preindustrial to present-day. Most models do not simulate the decreasing trend of BC from the 1950s to the 1970s that is measured in the Tibetan Plateau. As pointed out by Xu et al. (2009a), this decreasing trend reflects a strong influence of the Western European emissions to this region; Western European BC emissions declined after the peak in the 1930s. The increasing trend in models after the 1950s is consistent with emission increases in the neighboring regions including Eastern Europe, the Middle East, South Asia and East Asia. Without the high concentrations in the 1950s–1960s, some models simulated the observed magnitudes well except at Zuoqiupu and Rongbuk. Although models severely underestimate BC concentrations at Zuoqiupu, models successfully capture higher BC concentrations during the non-monsoon season than monsoon season. For the Greenland ice

ACPD
12, 21713–21778, 2012

core records, models follow the observed temporal patterns quite well, with the maximum around the 1930s, and capture the similar magnitude as the observation. However, compare to the decreasing trend after the 1950s in the ice core records, modeled BC concentrations show either much slower decrease or no decrease. Finally, models tend to capture the temporal trends seen in the Alps ice core records (i.e. two ice core records from the Colle Gnifetti glacier and one from the Fiescherhorn glacier), although some discrepancy is observed between two BC ice core records from the Colle Gnifetti glacier possibly due to different measurement technique. Both simulated and observed temporal trends indicate a strong influence from Europe.

Globally annually averaged BC albedo forcing from the offline NCAR Community models ranges from 0.014 $W m^{-2}$ to 0.019 $W m^{-2}$ in 2000 relative to 1850 among the ACCMIP models. This is smaller than previously reported forcing (Flanner et al., 2007) because of our method to compute the forcing; the offline method leads to less snow cover over the Tibetan Plateau and other portions of Asia, where Flanner et al. (2007) estimated large positive forcing. For spatially distributed BC albedo forcing in 2000, we estimated strong positive everywhere with high forcing (i.e. over 0.1 $W m^{-2}$) over Manchuria, Karakoram, and most of the Former USSR. Models predict the highest global annual average BC forcing in 1980 rather than 2000 mostly because of the higher FF/BF emissions in the Former USSR in 1980 compared to 2000. Interestingly, despite the similarity between Lamarque et al. (2010) and Bond et al. (2007), we find that the global annual average BC albedo forcing is higher in 1930 than in 1980 when using Bond et al. (2007). This is based on the comparison between the ACCMIP simulations in CICERO-OsloCTM2 and results from Skeie et al. (2011).

For GISS-E2-R, GISS-E2-R-TOMAS, and CICERO-OsloCTM2, we compare our offline BC albedo forcing to the online BC albedo forcing computed in its own model. They can differ by up to a factor of 2, revealing how the BC-snow parameterizations and model snow cover impact BC albedo forcing. Global annual average BC albedo forcing from two different GISS models varies from 0.015 $W m^{-2}$ (GISS-E-2-R) to 0.019 $W m^{-2}$ (GISS-E2-R-TOMAS) with our offline forcing but from 0.009 $W m^{-2}$

ACPD
12, 21713–21778, 2012

(GISS-E-2-R) and 0.022 $W m^{-2}$ (GISS-E2-R-TOMAS) with the online forcing computed in the GISS GCM. Given the main difference in the two GISS models is aerosol representation (i.e. GISS-E2-R with no microphysics and GISS-E2-R-TOMAS with sectional aerosol microphysics model), this suggests that different aerosol modeling can lead to approximately a factor of two difference.

Supplementary material related to this article is available online at: http://www.atmos-chem-phys-discuss.net/12/21713/2012/acpd-12-21713-2012-supplement.pdf.

Acknowledgements. ACCMIP is organized under the auspices of Atmospheric Chemistry and Climate (AC&C), a project of International Global Atmospheric Chemistry (IGAC) and Stratospheric Processes And their Role in Climate (SPARC) under the International Geosphere-Biosphere Project (IGBP) and World Climate Research Program (WCRP). The authors are thankful to the British Atmospheric Data Centre (BADC), which is part of the NERC National Centre for Atmospheric Science (NCAS), for collecting and archiving the ACCMIP data. Y. H. Lee, D. T. Shindell, and G. Faluvegi acknowledges support of the NASA MAP and ACMAP programs. V. Naik and L. W. Horowitz acknowledge efforts of GFDL's Global Atmospheric Model Development Team in the development of the GFDL-AM3 and Modeling Services Group for assistance with data processing. S. Ghan was supported by the US Department of Energy Office of Science Decadal and Regional Climate Prediction using Earth System Models (EaSM) program. The Pacific Northwest National Laboratory (PNNL) is operated for the Department of Energy (DOE) by Battelle Memorial Institute under contract DE-AC06-76RLO 1830. W. J. Collins and S. T. Rumbold were supported by the Joint DECC and Defra Integrated Climate Programme (GA01101). The CICERO-OsloCTM2 simulations were done within the projects SLAC (Short Lived Atmospheric Components) and EarthClim funded by the Norwegian Research Council. The CESM project, including NCAR-CAM3.5, is supported by the National Science Foundation and the Office of Science (BER) of the US Department of Energy. The National Center for Atmospheric Research is operated by the University Corporation for Atmospheric Research under sponsorship of the National Science Foundation. The MIROC-CHEM calculations were

ACPD
12, 21713–21778, 2012

performed on the NIES supercomputer system (NEC SX-8R), and supported by the Environment Research and Technology Development Fund (S-7) of the Ministry of the Environment, Japan.

The authors would like to thank NOAA-ESRL-GMD aerosol group, Norwegian Institute for Air Research (NILU), Atmospheric Radiation Measurement (ARM) Climate Research Facility operated for DOE, Sangeeta Sharma (Environment Canada), Heikki Lihavainen (Finnish Meteorological Institute), Sandy Starkweather (NOAA), Ernest Weingartner (Paul Scherrer Institute) and Martine Collaud Coen (MeteoSwiss) for providing BC surface mass concentration data. Special thanks to Betsy Andrews at NOAA and Ann Mari Fjæraa at NILU for helping us to obtain several BC surface mass concentrations dataset. We thank the EUSAAR-ACTRIS network for sampling BC at several EMEP stations. S. G. Jennings and Colin O'Dowd, Centre for Climate and Air Pollution Studies, School of Physics, National University of Ireland Galway are acknowledged for the use of surface black carbon data taken at the Mace Head Atmospheric Research Station on the west coast of Ireland. We also acknowledge the contribution of aethalometer BC data from Zeppelin, Ny-Alesund by K. Eleftheriadis, NCSR Demokritos and the support of NILU and Norsk Polar Institute. Finally, special thanks to Stephen Warren (Dept. of Atmospheric Science, Univ. of Washington, Seattle, WA, USA) and Sarah Doherty (JISAO, Univ. of Washington, Seattle, WA, USA) for making available measurements of snow BC concentrations from the Arctic.

References

Ackerman, A. S., Toon, O. B., Stevens, D. E., Heymsfield, A. J., Ramanathan, V., and Welton, E. J.: Reduction of tropical cloudiness by soot, Science, 288, 1042–1047, doi:10.1126/science.288.5468.1042, 2000.

Andrew, E., Ogren, J. A., Bonasoni, P., Marinoni, A., Cuevas, E., Rodriguez, S., Sun, J. Y., Jaffe, D. A., Fischer, E. V., Baltensperger, U., Weingartner, E., Coen, M. C., Sharma, S., Macdonald, A. M., Leaitch, W. R., Lin, N. H., Laj, P., Arsov, T., Kalapov, I., Jefferson, A., and Sheridan, P.: Climatology of aerosol radiative properties in the free troposphere, Atmos. Res., 102, 365–393, doi:10.1016/j.atmosres.2011.08.017, 2011.

Bauer, S. E., Wright, D. L., Koch, D., Lewis, E. R., McGraw, R., Chang, L.-S., Schwartz, S. E., and Ruedy, R.: MATRIX (Multiconfiguration Aerosol TRacker of mIXing state): an aerosol

ACPD

12, 21713–21778, 2012

microphysical module for global atmospheric models, Atmos. Chem. Phys., 8, 6003–6035, doi:10.5194/acp-8-6003-2008, 2008.
Bauer, S. E., and Menon, S.: Aerosol direct, indirect, semidirect, and surface albedo effects from sector contributions based on the IPCC AR5 emissions for preindustrial and present-day conditions, J. Geophys. Res.-Atmos., 117, D01206, doi:10.1029/2011jd016816, 2012.
Bellouin, N., Rae, J., Jones, A., Johnson, C., Haywood, J., and Boucher, O.: Aerosol forcing in the Climate Model Intercomparison Project (CMIP5) simulations by HadGEM2-ES and the role of ammonium nitrate, J. Geophys. Res.-Atmos., 116, D20206, doi:10.1029/2011jd016074, 2011.
Bisiaux, M. M., Edwards, R., McConnell, J. R., Albert, M. R., Anschütz, H., Neumann, T. A., Isaksson, E., and Penner, J. E.: Variability of black carbon deposition to the East Antarctic Plateau, 1800–2000 AD, Atmos. Chem. Phys., 12, 3799–3808, doi:10.5194/acp-12-3799-2012, 2012a.
Bisiaux, M. M., Edwards, R., McConnell, J. R., Curran, M. A. J., Van Ommen, T. D., Smith, A. M., Neumann, T. A., Pasteris, D. R., Penner, J. E., and Taylor, K.: Changes in black carbon deposition to Antarctica from two high-resolution ice core records, 1850–2000 AD, Atmos. Chem. Phys., 12, 4107–4115, doi:10.5194/acp-12-4107-2012, 2012b.
Bodhaine, B. A.: Aerosol absorption-measurements at Barrow, Mauna-Loa and the South-Pole, J. Geophys. Res.-Atmos., 100, 8967–8975, doi:10.1029/95jd00513, 1995.
Bond, T. C., Streets, D. G., Yarber, K. F., Nelson, S. M., Woo, J. H., and Klimont, Z.: A technology-based global inventory of black and organic carbon emissions from combustion, J. Geophys. Res.-Atmos., 109, D14203, doi:10.1029/2003JD003697, 2004.
Bond, T. C., Bhardwaj, E., Dong, R., Jogani, R., Jung, S. K., Roden, C., Streets, D. G., and Trautmann, N. M.: Historical emissions of black and organic carbon aerosol from energy-related combustion, 1850–2000, Global Biogeochem. Cy., 21, D14203, doi:10.1029/2006gb002840, 2007.
Browse, J., Carslaw, K. S., Arnold, S. R., Pringle, K., and Boucher, O.: The scavenging processes controlling the seasonal cycle in Arctic sulphate and black carbon aerosol, Atmos. Chem. Phys., 12, 6775–6798, doi:10.5194/acp-12-6775-2012, 2012.
Chaubey, J. P., Moorthy, K. K., Babu, S. S., Nair, V. S., and Tiwari, A.: Black carbon aerosols over coastal Antarctica and its scavenging by snow during the southern hemispheric summer, J. Geophys. Res.-Atmos., 115, D10210, doi:10.1029/2009jd013381, 2010.

ACPD
12, 21713–21778, 2012

Collaud Coen, M., Weingartner, E., Nyeki, S., Cozic, J., Henning, S., Verheggen, B., Gehrig, R., and Baltensperger, U.: Long-term trend analysis of aerosol variables at the high-alpine site Jungfraujoch, J. Geophys. Res.-Atmos., 112, D13213, doi:10.1029/2006jd007995, 2007.

Collaud Coen, M., Weingartner, E., Apituley, A., Ceburnis, D., Fierz-Schmidhauser, R., Flentje, H., Henzing, J. S., Jennings, S. G., Moerman, M., Petzold, A., Schmid, O., and Baltensperger, U.: Minimizing light absorption measurement artifacts of the Aethalometer: evaluation of five correction algorithms, Atmos. Meas. Tech., 3, 457–474, doi:10.5194/amt-3-457-2010, 2010.

Conway, H., Gades, A., and Raymond, C. F.: Albedo of dirty snow during conditions of melt, Water Resour. Res., 32, 1713–1718, doi:10.1029/96wr00712, 1996.

Cozic, J., Verheggen, B., Mertes, S., Connolly, P., Bower, K., Petzold, A., Baltensperger, U., and Weingartner, E.: Scavenging of black carbon in mixed phase clouds at the high alpine site Jungfraujoch, Atmos. Chem. Phys., 7, 1797–1807, doi:10.5194/acp-7-1797-2007, 2007.

Cozic, J., Mertes, S., Verheggen, B., Cziczo, D. J., Gallavardin, S. J., Walter, S., Baltensperger, U., and Weingartner, E.: Black carbon enrichment in atmospheric ice particle residuals observed in lower tropospheric mixed phase clouds, J. Geophys. Res.-Atmos., 113, D15209, doi:10.1029/2007jd009266, 2008.

Doherty, S. J., Warren, S. G., Grenfell, T. C., Clarke, A. D., and Brandt, R. E.: Light-absorbing impurities in Arctic snow, Atmos. Chem. Phys., 10, 11647–11680, doi:10.5194/acp-10-11647-2010, 2010.

Donner, L. J., Wyman, B. L., Hemler, R. S., Horowitz, L. W., Ming, Y., Zhao, M., Golaz, J. C., Ginoux, P., Lin, S. J., Schwarzkopf, M. D., Austin, J., Alaka, G., Cooke, W. F., Delworth, T. L., Freidenreich, S. M., Gordon, C. T., Griffies, S. M., Held, I. M., Hurlin, W. J., Klein, S. A., Knutson, T. R., Langenhorst, A. R., Lee, H. C., Lin, Y. L., Magi, B. I., Malyshev, S. L., Milly, P. C. D., Naik, V., Nath, M. J., Pincus, R., Ploshay, J. J., Ramaswamy, V., Seman, C. J., Shevliakova, E., Sirutis, J. J., Stern, W. F., Stouffer, R. J., Wilson, R. J., Winton, M., Wittenberg, A. T., and Zeng, F. R.: The dynamical core, physical parameterizations, and basic simulation characteristics of the atmospheric component AM3 of the GFDL global coupled model CM3, J. Climate, 24, 3484–3519, doi:10.1175/2011jcli3955.1, 2011.

Eleftheriadis, K., Vratolis, S., and Nyeki, S.: Aerosol black carbon in the European Arctic: measurements at Zeppelin station, Ny-Alesund, Svalbard from 1998–2007, Geophys. Res. Lett., 36, L02809, doi:10.1029/2008gl035741, 2009.

ACPD
12, 21713–21778, 2012

Fagerli, H., Legrand, M., Preunkert, S., Vestreng, V., Simpson, D., and Cerqueira, M.: Modeling historical long-term trends of sulfate, ammonium, and elemental carbon over Europe: a comparison with ice core records in the Alps, J. Geophys. Res.-Atmos., 112, D23s13, doi:10.1029/2006jd008044, 2007.

Flanner, M. G., Zender, C. S., Randerson, J. T., and Rasch, P. J.: Present-day climate forcing and response from black carbon in snow, J. Geophys. Res.-Atmos., 112, D11202, doi:10.1029/2006jd008003, 2007.

Flanner, M. G., Zender, C. S., Hess, P. G., Mahowald, N. M., Painter, T. H., Ramanathan, V., and Rasch, P. J.: Springtime warming and reduced snow cover from carbonaceous particles, Atmos. Chem. Phys., 9, 2481–2497, doi:10.5194/acp-9-2481-2009, 2009.

Gabrieli, J., Vallelonga, P., Cozzi, G., Gabrielli, P., Gambaro, A., Sigl, M., Decet, F., Schwikowski, M., Gaeggeler, H., Boutron, C., Cescon, P., and Barbante, C.: Post 17th-century changes of European PAH emissions recorded in high-altitude Alpine snow and ice, Environ. Sci. Technol., 44, 3260–3266, doi:10.1021/es903365s, 2010.

Garrett, T. J., Brattstrom, S., Sharma, S., Worthy, D. E. J., and Novelli, P.: The role of scavenging in the seasonal transport of black carbon and sulfate to the Arctic, Geophys. Res. Lett., 38, L16805, doi:10.1029/2011gl048221, 2011.

Gong, S. L., Zhao, T. L., Sharma, S., Toom-Sauntry, D., Lavoue, D., Zhang, X. B., Leaitch, W. R., and Barrie, L. A.: Identification of trends and interannual variability of sulfate and black carbon in the Canadian High Arctic: 1981–2007, J. Geophys. Res.-Atmos., 115, L16805, doi:10.1029/2009jd012943, 2010.

Graf, H.-F., Shirsat, S. V., Oppenheimer, C., Jarvis, M. J., Podzun, R., and Jacob, D.: Continental scale Antarctic deposition of sulphur and black carbon from anthropogenic and volcanic sources, Atmos. Chem. Phys., 10, 2457–2465, doi:10.5194/acp-10-2457-2010, 2010.

Hansen, J. and Nazarenko, L.: Soot climate forcing via snow and ice albedos, P. Natl. Acad. Sci. USA, 101, 423–428, doi:10.1073/pnas.2237157100, 2004.

Hegg, D. A., Warren, S. G., Grenfell, T. C., Doherty, S. J., Larson, T. V., and Clarke, A. D.: Source attribution of black carbon in Arctic snow, Environ. Sci. Technol., 43, 4016–4021, doi:10.1021/es803623f, 2009.

Hegg, D. A., Warren, S. G., Grenfell, T. C., Doherty, S. J., and Clarke, A. D.: Sources of light-absorbing aerosol in arctic snow and their seasonal variation, Atmos. Chem. Phys., 10, 10923–10938, doi:10.5194/acp-10-10923-2010, 2010.

ACPD
12, 21713–21778, 2012

Hirdman, D., Burkhart, J. F., Sodemann, H., Eckhardt, S., Jefferson, A., Quinn, P. K., Sharma, S., Ström, J., and Stohl, A.: Long-term trends of black carbon and sulphate aerosol in the Arctic: changes in atmospheric transport and source region emissions, Atmos. Chem. Phys., 10, 9351–9368, doi:10.5194/acp-10-9351-2010, 2010a.

Hirdman, D., Sodemann, H., Eckhardt, S., Burkhart, J. F., Jefferson, A., Mefford, T., Quinn, P. K., Sharma, S., Ström, J., and Stohl, A.: Source identification of short-lived air pollutants in the Arctic using statistical analysis of measurement data and particle dispersion model output, Atmos. Chem. Phys., 10, 669-693, doi:10.5194/acp-10-669-2010, 2010b.

Holland, M. M., Bailey, D. A., Briegleb, B. P., Light, B., and Hunke, E.: Improved sea ice shortwave radiation physics in CCSM4: the impact of melt ponds and aerosols on Arctic sea ice, J. Climate, 25, 1413–1430, doi:10.1175/jcli-d-11-00078.1, 2012.

Huang, L., Gong, S. L., Jia, C. Q., and Lavoue, D.: Relative contributions of anthropogenic emissions to black carbon aerosol in the Arctic, J. Geophys. Res.-Atmos., 115, D19208, doi:10.1029/2009jd013592, 2010a.

Huang, L., Gong, S. L., Jia, C. Q., and Lavoue, D.: Importance of deposition processes in simulating the seasonality of the Arctic black carbon aerosol, J. Geophys. Res.-Atmos., 115, D17207, doi:10.1029/2009jd013478, 2010b.

Hyvarinen, A. P., Kolmonen, P., Kerminen, V. M., Virkkula, A., Leskinen, A., Komppula, M., Hatakka, J., Burkhart, J., Stohl, A., Aalto, P., Kulmala, M., Lehtinen, K. E. J., Viisanen, Y., and Lihavainen, H.: Aerosol black carbon at five background measurement sites over Finland, a gateway to the Arctic, Atmos. Environ., 45, 4042–4050, doi:10.1016/j.atmosenv.2011.04.026, 2011.

Jacobson, M. Z.: Climate response of fossil fuel and biofuel soot, accounting for soot's feedback to snow and sea ice albedo and emissivity, J. Geophys. Res.-Atmos., 109, D21201, doi:10.1029/2004jd004945, 2004.

Jacobson, M. Z.: Short-term effects of controlling fossil-fuel soot, biofuel soot and gases, and methane on climate, Arctic ice, and air pollution health, J. Geophys. Res.-Atmos., 115, D14209, doi:10.1029/2009jd013795, 2010.

Jenk, T. M., Szidat, S., Schwikowski, M., Gäggeler, H. W., Brütsch, S., Wacker, L., Synal, H.-A., and Saurer, M.: Radiocarbon analysis in an Alpine ice core: record of anthropogenic and biogenic contributions to carbonaceous aerosols in the past (1650–1940), Atmos. Chem. Phys., 6, 5381–5390, doi:10.5194/acp-6-5381-2006, 2006.

ACPD
12, 21713–21778, 2012

Jiao, C., Flanner, M., et al.: Multi-model assessment of black carbon in Arctic snow and sea-ice: an AeroCom analysis, in preparation, 2012.
Junker, C., Jennings, S. G., and Cachier, H.: Aerosol light absorption in the North Atlantic: trends and seasonal characteristics during the period 1989 to 2003, Atmos. Chem. Phys., 6, 1913–1925, doi:10.5194/acp-6-1913-2006, 2006.
Kaspari, S. D., Schwikowski, M., Gysel, M., Flanner, M. G., Kang, S., Hou, S., and Mayewski, P. A.: Recent increase in black carbon concentrations from a Mt. Everest ice core spanning 1860–2000 AD, Geophys. Res. Lett., 38, L04703, doi:10.1029/2010gl046096, 2011.
Kehrwald, N. M., Thompson, L. G., Yao, T. D., Mosley-Thompson, E., Schotterer, U., Alfimov, V., Beer, J., Eikenberg, J., and Davis, M. E.: Mass loss on Himalayan glacier endangers water resources, Geophys. Res. Lett., 35, L22503, doi:10.1029/2008gl035556, 2008.
Koch, D. and Hansen, J.: Distant origins of Arctic black carbon: a Goddard Institute for Space Studies ModelE experiment, J. Geophys. Res.-Atmos., 110, D04204, doi:10.1029/2004jd005296, 2005.
Koch, D. and Del Genio, A. D.: Black carbon semi-direct effects on cloud cover: review and synthesis, Atmos. Chem. Phys., 10, 7685–7696, doi:10.5194/acp-10-7685-2010, 2010.
Koch, D., Menon, S., Del Genio, A., Ruedy, R., Alienov, I., and Schmidt, G. A.: Distinguishing aerosol impacts on climate over the past century, J. Climate, 22, 2659–2677, doi:10.1175/2008jcli2573.1, 2009a.
Koch, D., Schulz, M., Kinne, S., McNaughton, C., Spackman, J. R., Balkanski, Y., Bauer, S., Berntsen, T., Bond, T. C., Boucher, O., Chin, M., Clarke, A., De Luca, N., Dentener, F., Diehl, T., Dubovik, O., Easter, R., Fahey, D. W., Feichter, J., Fillmore, D., Freitag, S., Ghan, S., Ginoux, P., Gong, S., Horowitz, L., Iversen, T., Kirkevåg, A., Klimont, Z., Kondo, Y., Krol, M., Liu, X., Miller, R., Montanaro, V., Moteki, N., Myhre, G., Penner, J. E., Perlwitz, J., Pitari, G., Reddy, S., Sahu, L., Sakamoto, H., Schuster, G., Schwarz, J. P., Seland, Ø., Stier, P., Takegawa, N., Takemura, T., Textor, C., van Aardenne, J. A., and Zhao, Y.: Evaluation of black carbon estimations in global aerosol models, Atmos. Chem. Phys., 9, 9001–9026, doi:10.5194/acp-9-9001-2009, 2009b.
Koch, D., Bauer, S. E., Del Genio, A., Faluvegi, G., McConnell, J. R., Menon, S., Miller, R. L., Rind, D., Ruedy, R., Schmidt, G. A., and Shindell, D.: Coupled aerosol-chemistry-climate twentieth-century transient model investigation: trends in short-lived species and climate responses, J. Climate, 24, 2693–2714, doi:10.1175/2011jcli3582.1, 2011.

ACPD
12, 21713–21778, 2012

Kopacz, M., Mauzerall, D. L., Wang, J., Leibensperger, E. M., Henze, D. K., and Singh, K.: Origin and radiative forcing of black carbon transported to the Himalayas and Tibetan Plateau, Atmos. Chem. Phys., 11, 2837–2852, doi:10.5194/acp-11-2837-2011, 2011.

Kopp, R. E. and Mauzerall, D. L.: Assessing the climatic benefits of black carbon mitigation, P. Natl. Acad. Sci. USA, 107, 11703–11708, doi:10.1073/pnas.0909605107, 2010.

Lamarque, J.-F., Bond, T. C., Eyring, V., Granier, C., Heil, A., Klimont, Z., Lee, D., Liousse, C., Mieville, A., Owen, B., Schultz, M. G., Shindell, D., Smith, S. J., Stehfest, E., Van Aardenne, J., Cooper, O. R., Kainuma, M., Mahowald, N., McConnell, J. R., Naik, V., Riahi, K., and van Vuuren, D. P.: Historical (1850–2000) gridded anthropogenic and biomass burning emissions of reactive gases and aerosols: methodology and application, Atmos. Chem. Phys., 10, 7017–7039, doi:10.5194/acp-10-7017-2010, 2010.

Lamarque, J.-F., Shindell, D. T., Josse, B., Eyring, V., Young, P. J., Cionni, I., Bergmann, D., Cameron-Smith, P., Collins, W. J., Doherty, R., Dalsoren, S., Faluvegi, G., Folberth, G., Ghan, S. J., Horowitz, L. W., Lee, Y. H., McKenzie, I., Nagashima, T., Naik, V., Plummer, D., Rumbold, S., Skeie, R., Stevenson, D. S., Strode, S., Sudo, K., Szopa, S., Voulgarikis, A., and Zeng, G.: The Atmospheric Chemistry and Climate Model Intercomparison Project (ACCMIP): overview and description of models, simulations and climate diagnostics, Atmos. Chem. Phys. Discuss., accepted, 2012a.

Lamarque, J.-F., Emmons, L. K., Hess, P. G., Kinnison, D. E., Tilmes, S., Vitt, F., Heald, C. L., Holland, E. A., Lauritzen, P. H., Neu, J., Orlando, J. J., Rasch, P. J., and Tyndall, G. K.: CAM-chem: description and evaluation of interactive atmospheric chemistry in the Community Earth System Model, Geosci. Model Dev., 5, 369–411, doi:10.5194/gmd-5-369-2012, 2012b.

Lavanchy, V. M. H., Gaggeler, H. W., Schotterer, U., Schwikowski, M., and Baltensperger, U.: Historical record of carbonaceous particle concentrations from a European high-alpine glacier (Colle Gnifetti, Switzerland), J. Geophys. Res.-Atmos., 104, 21227–21236, doi:10.1029/1999jd900408, 1999.

Law, K. S. and Stohl, A.: Arctic air pollution: origins and impacts, Science, 315, 1537–1540, doi:10.1126/science.1137695, 2007.

Lawrence, D. M., Oleson, K. W., Flanner, M., Thornton, P., Swenson, S. C., Lawrence, P., Zeng, X., Yang, Z., Levis, S., Sakaguchi, K., Bonan, G. B., and Slater, A.: Parameterization improvements and functional and structural advances in version 4 of the Community Land Model, J. Adv. Model. Earth Syst., 3, M03001, doi:10.1029/2011MS000045, 2011.

ACPD
12, 21713–21778, 2012

Lawrence, D. M., Oleson, K. W., Flanner, M. G., Fletcher, C. G., Lawrence, P. J., Levis, S., Swenson, S. C., and Bonan, G. B.: The CCSM4 land simulation, 1850–2005: assessment of surface climate and new capabilities, J. Climate, 25, 2240–2260, doi:10.1175/jcli-d-11-00103.1, 2012.

Lee, Y. H. and Adams, P. J.: A fast and efficient version of the TwO-Moment Aerosol Sectional (TOMAS) global aerosol microphysics model, Aerosol Sci. Tech., 46, 678–689, doi:10.1080/02786826.2011.643259, 2011.

Liu, J. F., Fan, S. M., Horowitz, L. W., and Levy, H.: Evaluation of factors controlling long-range transport of black carbon to the Arctic, J. Geophys. Res.-Atmos., 116, D04307, doi:10.1029/2010jd015145, 2011.

Liu, X., Easter, R. C., Ghan, S. J., Zaveri, R., Rasch, P., Shi, X., Lamarque, J.-F., Gettelman, A., Morrison, H., Vitt, F., Conley, A., Park, S., Neale, R., Hannay, C., Ekman, A. M. L., Hess, P., Mahowald, N., Collins, W., Iacono, M. J., Bretherton, C. S., Flanner, M. G., and Mitchell, D.: Toward a minimal representation of aerosols in climate models: description and evaluation in the Community Atmosphere Model CAM5, Geosci. Model Dev., 5, 709–739, doi:10.5194/gmd-5-709-2012, 2012.

Lu, Z., Streets, D. G., Zhang, Q., and Wang, S.: A novel back-trajectory analysis of the origin of black carbon transported to the Himalayas and Tibetan Plateau during 1996–2010, Geophys. Res. Lett., 39, L01809, doi:10.1029/2011gl049903, 2012.

Lubin, D. and Vogelmann, A. M.: A climatologically significant aerosol longwave indirect effect in the Arctic, Nature, 439, 453–456, doi:10.1038/nature04449, 2006.

Lund, M. T. and Berntsen, T.: Parameterization of black carbon aging in the OsloCTM2 and implications for regional transport to the Arctic, Atmos. Chem. Phys., 12, 6999–7014, doi:10.5194/acp-12-6999-2012, 2012.

McConnell, J. R.: New Directions: historical black carbon and other ice core aerosol records in the Arctic for GCM evaluation, Atmos. Environ., 44, 2665–2666, doi:10.1016/j.atmosenv.2010.04.004, 2010.

McConnell, J. R. and Edwards, R.: Coal burning leaves toxic heavy metal legacy in the Arctic, P. Natl. Acad. Sci. USA, 105, 12140–12144, doi:10.1073/pnas.0803564105, 2008.

McConnell, J. R., Edwards, R., Kok, G. L., Flanner, M. G., Zender, C. S., Saltzman, E. S., Banta, J. R., Pasteris, D. R., Carter, M. M., and Kahl, J. D. W.: 20th-century industrial black carbon emissions altered arctic climate forcing, Science, 317, 1381–1384, doi:10.1126/science.1144856, 2007.

ACPD

12, 21713–21778, 2012

Mieville, A., Granier, C., Liousse, C., Guillaume, B., Mouillot, F., Lamarque, J. F., Gregoire, J. M., and Petron, G.: Emissions of gases and particles from biomass burning during the 20th century using satellite data and an historical reconstruction, Atmos. Environ., 44, 1469–1477, doi:10.1016/j.atmosenv.2010.01.011, 2010.

Ming, J., Cachier, H., Xiao, C., Qin, D., Kang, S., Hou, S., and Xu, J.: Black carbon record based on a shallow Himalayan ice core and its climatic implications, Atmos. Chem. Phys., 8, 1343–1352, doi:10.5194/acp-8-1343-2008, 2008.

Moosmuller, H., Chakrabarty, R. K., and Arnott, W. P.: Aerosol light absorption and its measurement: a review, J. Quant. Spectrosc. Ra., 110, 844–878, doi:10.1016/j.jqsrt.2009.02.035, 2009.

Qian, T., Dai, A., Trenberth, K. E., and Oleson, K. W.: Simulation of global land surface conditions from 1948 to 2004. Part I: Forcing data and evaluations, J. Hydrometeorol., 7, 953–975, doi:10.1175/jhm540.1, 2006.

Quinn, P. K., Shaw, G., Andrews, E., Dutton, E. G., Ruoho-Airola, T., and Gong, S. L.: Arctic haze: current trends and knowledge gaps, Tellus B, 59, 99–114, doi:10.1111/j.1600-0889.2006.00238.x, 2007.

Quinn, P. K., Bates, T. S., Baum, E., Doubleday, N., Fiore, A. M., Flanner, M., Fridlind, A., Garrett, T. J., Koch, D., Menon, S., Shindell, D., Stohl, A., and Warren, S. G.: Short-lived pollutants in the Arctic: their climate impact and possible mitigation strategies, Atmos. Chem. Phys., 8, 1723-1735, doi:10.5194/acp-8-1723-2008, 2008.

Reisinger, P., Wonaschuetz, A., Hitzenberger, R., Petzold, A., Bauer, H., Jankowski, N., Puxbaum, H., Chi, X., and Maenhaut, W.: Intercomparison of measurement techniques for black or elemental carbon under urban background conditions in wintertime: influence of biomass combustion, Environ. Sci. Technol., 42, 884–889, doi:10.1021/es0715041, 2008.

Schultz, M. G., Heil, A., Hoelzemann, J. J., Spessa, A., Thonicke, K., Goldammer, J. G., Held, A. C., Pereira, J. M. C., and van het Bolscher, M.: Global wildland fire emissions from 1960 to 2000, Global Biogeochem. Cy., 22, L01809, doi:10.1029/2007gb003031, 2008.

Sessions, W. R., Fuelberg, H. E., Kahn, R. A., and Winker, D. M.: An investigation of methods for injecting emissions from boreal wildfires using WRF-Chem during ARCTAS, Atmos. Chem. Phys., 11, 5719–5744, doi:10.5194/acp-11-5719-2011, 2011.

Sharma, S., Brook, J. R., Cachier, H., Chow, J., Gaudenzi, A., and Lu, G.: Light absorption and thermal measurements of black carbon in different regions of Canada, J. Geophys. Res.-Atmos., 107, 4771, doi:10.1029/2002jd002496, 2002.

ACPD
12, 21713–21778, 2012

Sharma, S., Lavoue, D., Cachier, H., Barrie, L. A., and Gong, S. L.: Long-term trends of the black carbon concentrations in the Canadian Arctic, J. Geophys. Res.-Atmos., 109, D15203, doi:10.1029/2003jd004331, 2004.

Shindell, D. T., Chin, M., Dentener, F., Doherty, R. M., Faluvegi, G., Fiore, A. M., Hess, P., Koch, D. M., MacKenzie, I. A., Sanderson, M. G., Schultz, M. G., Schulz, M., Stevenson, D. S., Teich, H., Textor, C., Wild, O., Bergmann, D. J., Bey, I., Bian, H., Cuvelier, C., Duncan, B. N., Folberth, G., Horowitz, L. W., Jonson, J., Kaminski, J. W., Marmer, E., Park, R., Pringle, K. J., Schroeder, S., Szopa, S., Takemura, T., Zeng, G., Keating, T. J., and Zuber, A.: A multi-model assessment of pollution transport to the Arctic, Atmos. Chem. Phys., 8, 5353–5372, doi:10.5194/acp-8-5353-2008, 2008.

Shindell, D. T., Lamarque, J.-F., Schulz, M., Flanner, M., Jiao, C., Chin, M., Young, P., Lee, Y. H., Rotstayn, L., Milly, G., Faluvegi, G., Balkanski, Y., Collins, W. J., Conley, A. J., Dalsoren, S., Easter, R., Ghan, S., Horowitz, L., Liu, X., Myhre, G., Nagashima, T., Naik, V., Rumbold, S., Skeie, R., Sudo, K., Szopa, S., Takemura, T., Voulgarakis, A., and Yoon, J.-H.: Radiative forcing in the ACCMIP historical and future climate simulations, Atmos. Chem. Phys. Discuss., 12, 21105–21210, doi:10.5194/acpd-12-21105-2012, 2012.

Skeie, R. B., Berntsen, T., Myhre, G., Pedersen, C. A., Ström, J., Gerland, S., and Ogren, J. A.: Black carbon in the atmosphere and snow, from pre-industrial times until present, Atmos. Chem. Phys., 11, 6809–6836, doi:10.5194/acp-11-6809-2011, 2011.

Stohl, A.: Characteristics of atmospheric transport into the Arctic troposphere, J. Geophys. Res.-Atmos., 111, D11306, doi:10.1029/2005jd006888, 2006.

Takemura, T., Okamoto, H., Maruyama, Y., Numaguti, A., Higurashi, A., and Nakajima, T.: Global three-dimensional simulation of aerosol optical thickness distribution of various origins, J. Geophys. Res.-Atmos., 105, 17853–17873, doi:10.1029/2000jd900265, 2000.

Takemura, T., Nakajima, T., Dubovik, O., Holben, B. N., and Kinne, S.: Single-scattering albedo and radiative forcing of various aerosol species with a global three-dimensional model, J. Climate, 15, 333–352, doi:10.1175/1520-0442(2002)015<0333:ssaarf>2.0.co;2, 2002.

Takemura, T., Nozawa, T., Emori, S., Nakajima, T. Y., and Nakajima, T.: Simulation of climate response to aerosol direct and indirect effects with aerosol transport-radiation model, J. Geophys. Res.-Atmos., 110, D02202, doi:10.1029/2004jd005029, 2005.

Textor, C., Schulz, M., Guibert, S., Kinne, S., Balkanski, Y., Bauer, S., Berntsen, T., Berglen, T., Boucher, O., Chin, M., Dentener, F., Diehl, T., Easter, R., Feichter, H., Fillmore, D., Ghan, S., Ginoux, P., Gong, S., Grini, A., Hendricks, J., Horowitz, L., Huang, P., Isaksen, I., Iversen, I.,

ACPD
12, 21713–21778, 2012

Kloster, S., Koch, D., Kirkevåg, A., Kristjansson, J. E., Krol, M., Lauer, A., Lamarque, J. F., Liu, X., Montanaro, V., Myhre, G., Penner, J., Pitari, G., Reddy, S., Seland, Ø., Stier, P., Takemura, T., and Tie, X.: Analysis and quantification of the diversities of aerosol life cycles within AeroCom, Atmos. Chem. Phys., 6, 1777–1813, doi:10.5194/acp-6-1777-2006, 2006.

Thevenon, F., Anselmetti, F. S., Bernasconi, S. M., and Schwikowski, M.: Mineral dust and elemental black carbon records from an Alpine ice core (Colle Gnifetti glacier) over the last millennium, J. Geophys. Res.-Atmos., 114, D17102, doi:10.1029/2008jd011490, 2009.

van der Werf, G. R., Randerson, J. T., Giglio, L., Collatz, G. J., Kasibhatla, P. S., and Arellano Jr., A. F.: Interannual variability in global biomass burning emissions from 1997 to 2004, Atmos. Chem. Phys., 6, 3423–3441, doi:10.5194/acp-6-3423-2006, 2006.

Vignati, E., Karl, M., Krol, M., Wilson, J., Stier, P., and Cavalli, F.: Sources of uncertainties in modelling black carbon at the global scale, Atmos. Chem. Phys., 10, 2595–2611, doi:10.5194/acp-10-2595-2010, 2010.

Wang, H., Easter, R. C., Rasch, P. J., Wang, M., Liu, X., Ghan, S. J., Qian, Y., Yoon, J.-H., Ma, P.-L., and Velu, V.: Improving aerosol transport to high-latitudes in the Community Atmosphere Model CAM5, J. Geophys. Res., submitted, 2012.

Wang, Q., Jacob, D. J., Fisher, J. A., Mao, J., Leibensperger, E. M., Carouge, C. C., Le Sager, P., Kondo, Y., Jimenez, J. L., Cubison, M. J., and Doherty, S. J.: Sources of carbonaceous aerosols and deposited black carbon in the Arctic in winter-spring: implications for radiative forcing, Atmos. Chem. Phys., 11, 12453-12473, doi:10.5194/acp-11-12453-2011, 2011.

Wang, Z. L., Zhang, H., and Shen, X. S.: Radiative forcing and climate response due to black carbon in snow and ice, Adv. Atmos. Sci., 28, 1336–1344, doi:10.1007/s00376-011-0117-5, 2011b.

Warneke, C., Froyd, K. D., Brioude, J., Bahreini, R., Brock, C. A., Cozic, J., de Gouw, J. A., Fahey, D. W., Ferrare, R., Holloway, J. S., Middlebrook, A. M., Miller, L., Montzka, S., Schwarz, J. P., Sodemann, H., Spackman, J. R., and Stohl, A.: An important contribution to springtime Arctic aerosol from biomass burning in Russia, Geophys. Res. Lett., 37, L01801, doi:10.1029/2009gl041816, 2010.

Watson, J. G., Chow, J. C., and Chen, L.-W. A.: Summary of organic and elemental carbon/black carbon analysis methods and intercomparisons, Aerosol Air Qual. Res., 5, 65–102, 2005.

ACPD
12, 21713–21778, 2012

Weingartner, E., Saathoff, H., Schnaiter, M., Streit, N., Bitnar, B., and Baltensperger, U.: Absorption of light by soot particles: determination of the absorption coefficient by means of aethalometers, J. Aerosol Sci., 34, 1445–1463, doi:10.1016/s0021-8502(03)00359-8, 2003.

Xu, B., Cao, J., Hansen, J., Yao, T., Joswia, D. R., Wang, N., Wu, G., Wang, M., Zhao, H., Yang, W., Liu, X., and He, J.: Black soot and the survival of Tibetan glaciers, P. Natl. Acad. Sci. USA, 106, 22114–22118, doi:10.1073/pnas.0910444106, 2009a.

Xu, J. C., Grumbine, R. E., Shrestha, A., Eriksson, M., Yang, X. F., Wang, Y., and Wilkes, A.: The melting Himalayas: cascading effects of climate change on water, biodiversity, and livelihoods, Conserv. Biol., 23, 520–530, doi:10.1111/j.1523-1739.2009.01237.x, 2009b.

Xu, B., Cao, J., Joswiak, D. R., Liu, X., Zhao, H., and He, J.: Post-depositional enrichment of black soot in snow-pack and accelerated melting of Tibetan glaciers, Environ. Res. Lett., 7, L01801, doi:10.1088/1748-9326/7/1/014022, 2012.

Yasunari, T. J., Bonasoni, P., Laj, P., Fujita, K., Vuillermoz, E., Marinoni, A., Cristofanelli, P., Duchi, R., Tartari, G., and Lau, K.-M.: Estimated impact of black carbon deposition during pre-monsoon season from Nepal Climate Observatory – Pyramid data and snow albedo changes over Himalayan glaciers, Atmos. Chem. Phys., 10, 6603–6615, doi:10.5194/acp-10-6603-2010, 2010.

ACPD
12, 21713–21778, 2012

Table 1. Model BC output availability in CMIP5 transient and ACCMIP timeslice historical runs used in this study. The core ACCMIP timeslice runs are shown with (core). "x" means model output is available for the corresponding year.

Model	CMIP5	ACCMIP timeslice runs								
	transient 1850–2005	1850 (core)	1890	1910	1930 (core)	1950	1970	1980 (core)	1990	2000 (core)
GISS-E2-R	x									
GISS-E2-R-TOMAS		x			x			x		x
GFDL-AM3		x*						x		x
CICERO-OsloCTM2		x		x	x		x	x	x	x
HadGEM2		x*						x		x
NCAR-CAM5.1		x	x	x	x	x	x	x	x	x
NCAR-CAM3.5	x	x			x			x		x
MIROC-CHEM	x	x			x			x		x

* GFDL-AM3 and HadGEM2 runs 1860 timeslice instead of 1850.

ACPD
12, 21713–21778, 2012

Table 2. BC modeling methodology. SF_{BC} standards for in-cloud scavenging fraction of hydrophilic BC. FF is for fossil fuel emissions; BF for biofuel emissions; BB for biomass burning emissions.

Model	Emission			Deposition		BC aging	Aerosol	Reference for
	Hydrophilic fraction	Injection height for BB	Mass median diameter	Dry deposition	Wet deposition for ice/mixed-phase clouds		microphysics	aerosol model
GISS-E2-R	0 %	within boundary layer (weighted by air mass in each layer)	n/a	resistance series	$0.012 \times SF_{BC}$	fixed 1 day e-folding (only FF/BF)	n/a	Koch et al. (2011)
GISS-E2-R-TOMAS	20 %	within boundary layer (weighted by air mass in each layer)	105.6 nm (FF), 422.6 nm (BB/BF)	resistance series	$0.012 \times SF_{BC}$	fixed 1.5 day e-folding	Sectional scheme	Lee and Adams (2011)
GFDL-AM3	20 %	up to 6 km (Dentener et al., 2006)	31 nm	empirical resistance method	as liquid clouds (i.e. $1.0 \times SF_{BC}$)	fixed 1.4 days e-folding	n/a	Donner et al. (2011)
CICERO-OsloCTM2	20 %	based on height distribution from the RETRO project	n/a	fixed over land and ocean depending on aerosol hygroscopity	Large-scale: $0.012 \times SF_{BC}$, Convective: $1.0 \times SF_{BC}$	dependence on latitude and season	n/a	Skeie et al. (2011); Lund and Berntsen (2012)
HadGEM2	0 % (FF/BF), 94.6 % (BB)	Homogenous in boundary layer	80 nm (FF/BF), 100 nm (BB)	resistance series	as liquid clouds (i.e. $1.0 \times SF_{BC}$)	fixed 1 day e-folding	mass-based modal scheme	Bellouin et al. (2007)
NCAR-CAM5.1	0 %	up to 6 km (Dentener et al., 2006)	134 nm	resistance series	n/a (warm couds only)	internally mixed with accumulation mode sulfate and organic	3 double-moment internally-mixed modes (modal scheme)	Liu et al. (2012)
NCAR-CAM3.5	20 %	into the surface layer	23.6 nm	0.1 $cm\,s^{-1}$ everywhere	n/a (warm couds only)	fixed 1.6 days e-folding	n/a	Lamarque et al. (2012b)
MIROC-CHEM	0 %	up to sigma = 0.75 (homogeneous mass mixing ratio)	78 nm (FF), 474 nm (BB/BF)	empirical resistance method	as liquid clouds (i.e. $1.0 \times SF_{BC}$)	n/a	n/a	Takemura et al. (2000, 2002, 2005)

ACPD
12, 21713–21778, 2012

Table 3. Global average BC budgets in 1850 and 2000 including emission, wet and dry deposition, burden, and lifetime.

Model	1850 (Preindustrial)					2000 (Present-day)				
	Emission (Tg)	Burden (Gg)	Wet deposition ($Tgyr^{-1}$)	Dry deposition ($Tgyr^{-1}$)	Lifetime (days)	Emission (Tg)	Burden (Gg)	Wet deposition ($Tgyr^{-1}$)	Dry deposition ($Tgyr^{-1}$)	Lifetime (days)
GISS-E2-R	4.0	55	2.9	1.0	5.1	8.8	138	6.3	2.3	5.8
GISS-E2-R-TOMAS	3.1	65	2.8	0.1	8.0	7.8	169	7.1	0.3	8.3
GFDL-AM3	3.1	53	2.8	0.3	6.2	7.8	131	3.8	3.4	6.6
CICERO-OsloCTM2	3.1	68	2.6	0.5	8.0	7.8	168	7.0	0.8	7.9
HadGEM2	3.1	103	2.6	0.5	12.3	7.8	315	6.1	1.4	15.2
NCAR-CAM5.1	3.1	34	2.6	0.5	4.0	7.8	82	6.5	1.2	3.9
NCAR-CAM3.5	3.1	50	2.4	0.7	5.9	7.8	126	6.1	1.8	5.9
MIROC-CHEM	3.0	37	2.5	0.3	4.8	7.7	111	6.1	1.0	5.7
multi-model mean	3.2	58	2.5	0.6	6.8	7.9	155	6.1	1.5	7.4
RSD	0.10	0.37	0.15	0.68	0.39	0.05	0.46	0.17	0.63	0.47

ACPD
12, 21713–21778, 2012

Table 4. List of observation sites for BC surface mass concentrations. Note that Ny-Ålesund and Hyytiälä are simply written as Ny-Alesund and Hyytiala, respectively, in the text and figures.

Site	Site category	Latitude	Longitude	Observation years	Observation method	Observed	Contributor
Alert	Arctic	83° N	297° W	1989 to 2006	Aethalometer	EBC	Sangeeta Sharma
Ny-Ålesund	Arctic	78.9° N	11.88° E	2005 to 2010	Aethalometer	EBC	EMEP/ebas (NILU)
Barrow	Arctic	71.3° N	156.6° W	1998 to 2011	PSAP	EBC	NOAA-ESRL-GMD
Pallas (Pallastunturi)	Sub-arctic	68° N	23.7° W	2005 to 2010	Aethalometer	EBC	Heikki Lihavainen
Hyytiälä	Remote Continental	61.85° N	24.28° E	2004 to 2011	Aethalometer	EBC	EMEP/ebas (NILU)
Preila	Continental Marine	55.35° N	21.07° E	2008 to 2010	Aethalometer	EBC	EMEP/ebas (NILU)
Mace Head	Remote Continental	53.17° N	9.5° W	2003 to 2007	Aethalometer	EBC	EMEP/ebas (NILU)
Jungfraujoch	Remote Continental	46.55° N	7.98° E	1995 to 2011	Aethalometer	EBC	Martine Collaud Coen
Ispra	Perturbed Continental (like urban background)	45.8° N	8.63° E	2007 to 2010	Filter absorption photometer	EBC	EMEP/ebas (NILU)
Sable Island	Perturbed Marine	43.93° N	299.99° W	1996 to 2000	PSAP	EBC	NOAA-ESRL-GMD
Trinidad Head	Continental Marine	41.05° N	235.85° W	2002 to 2011	PSAP	EBC	NOAA-ESRL-GMD
Bondville	Perturbed Continental	40.05° N	271.63° W	1996 to 2011	PSAP	EBC	NOAA-ESRL-GMD
Southern Great Plains	Perturbed Continental	36.61° N	262.51° W	1996 to 2011	PSAP	EBC	DOE-ARM/NOAA-ESRL-GMD
Mauna Loa	Marine, free troposphere	19.54° N	204.42° W	2001 to 2011	PSAP	EBC	NOAA-ESRL-GMD

ACPD
12, 21713–21778, 2012

Table 5. List of the BC ice core observation sites used in this study.

Regions	Site	Latitude	Longitude	Elevation (m)	Period	Data format	Contributor
Greenland	Humboldt	78.53° N	56.83° W	1985	1870 to 1992	deposition fluxes/concentrations	Joe McConnell
	Summit	72.6° N	38.3° W	3258	1871 to 2002	deposition fluxes/concentrations	Joe McConnell
	D4	71.4° N	43.9° W	2766	1872 to 2002	deposition fluxes/concentrations	Joe McConnell
	ACT2	66.00° N	45.2° W	2408	1873 to 2003	deposition fluxes/concentrations	Joe McConnell
Alps	Alps	45.92° N	7.87° E	4455	1433 to 1975	concentrations	Florian Thevenon
Tibetan Plateau	Mt. Muztagh Ata	38.28° N	75.10° E	6300	1955 to 2000	deposition fluxes/concentrations	Junji Cao
	Tanggula glacier	33.11° N	92.09° E	5800	1950 to 2004	deposition fluxes/concentrations	Junji Cao
	Zuoqiupun glacier	29.21° N	96.92° E	5600	1956 to 2006	deposition fluxes/concentrations	Junji Cao
	Nojin Kangsang glacier	29.04° N	90.2° E	5950	1950 to 2006	deposition fluxes/concentrations	Junji Cao
	Rongbuk glacier	28.02° N	86.96° E	6500	1975 to 2004	deposition fluxes/concentrations	Junji Cao
Antarctic	WAIS	79.47° S	112.09° W	1806	1850 to 2002	deposition fluxes/concentrations	Ross Edwards
	Law Dome	66.78° S	112.37° E	1230	1850 to 2001	deposition fluxes/concentrations	Marion Bisiaux/ Mark Curran

ACPD
12, 21713–21778, 2012

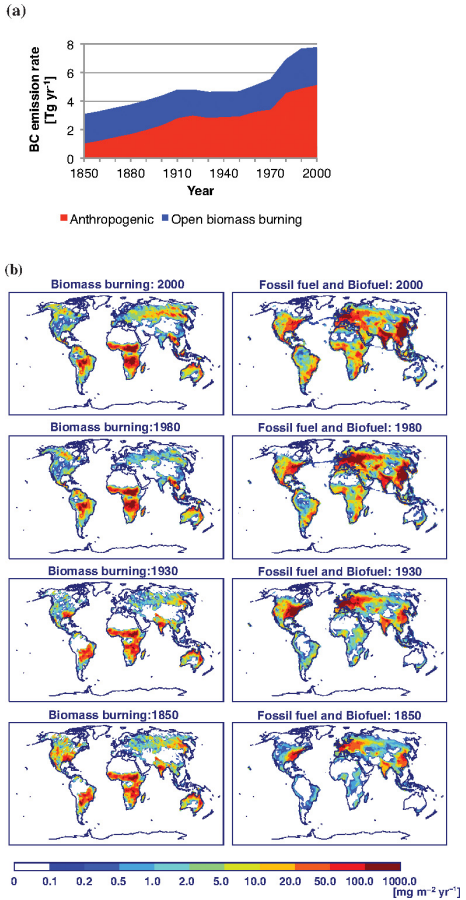

Fig. 1. Annual BC emission rate from 1850 to 2000. **(a)** is shown the global annual emission rate for Anthropogenic and open biomass burning, and **(b)** is its spatial distributions in 1850, 1930, 1980, and 2000.

ACPD
12, 21713–21778, 2012

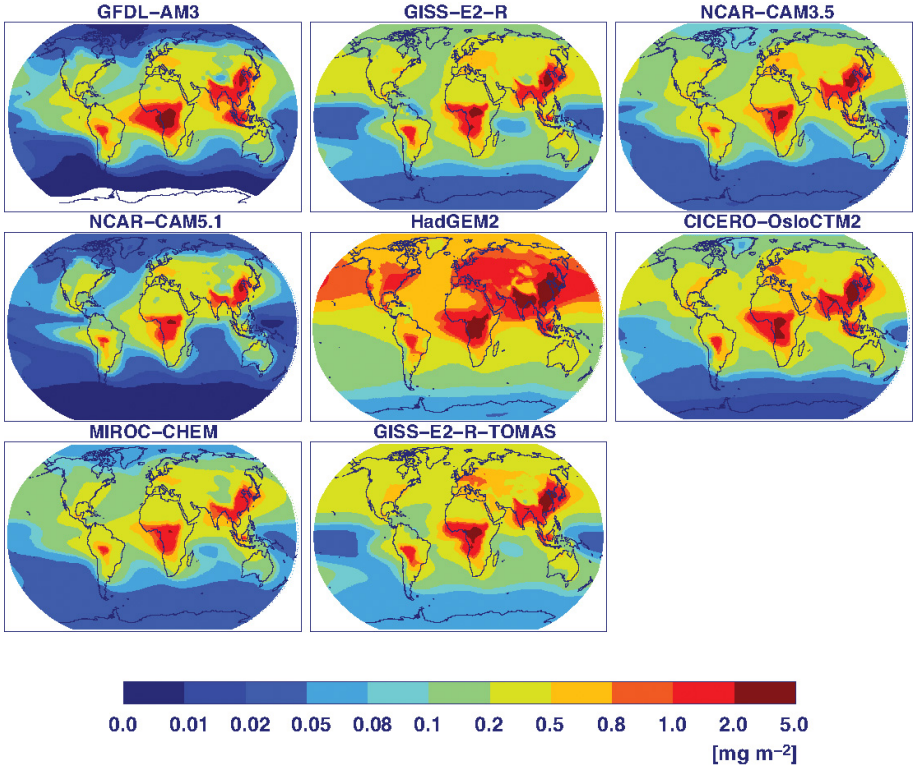

Fig. 2. Global distribution of BC column burden in 2000.

ACPD
12, 21713–21778, 2012

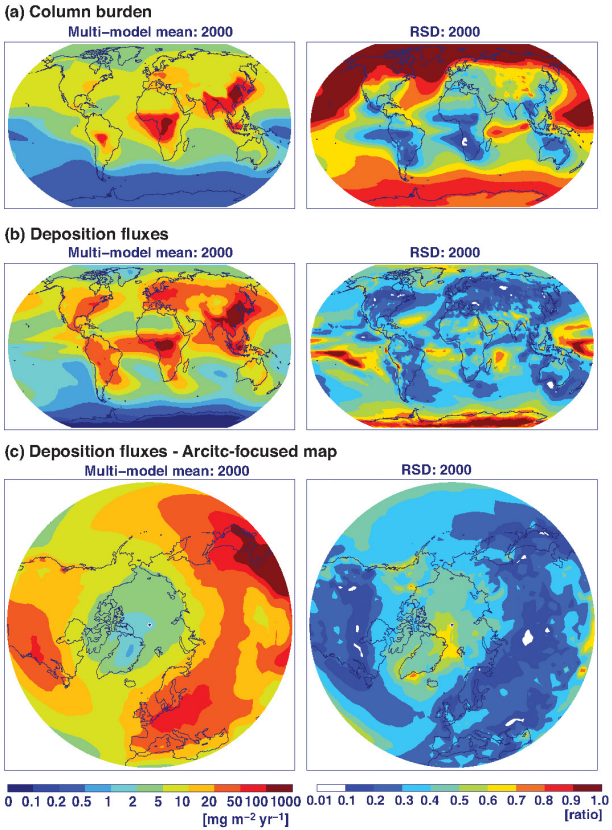

Fig. 3. Global distributions of the multi-model mean and RSD (relative standard deviation) of **(a)** BC column burden and **(b)** total BC deposition fluxes in 2000. **(c)** is same as **(b)** but with arctic-focused maps (latitude: 30° N to 90° N).

ACPD
12, 21713–21778, 2012

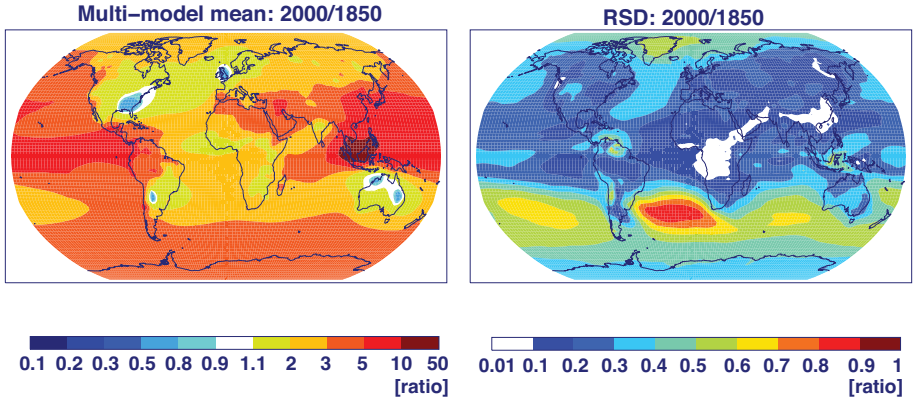

Fig. 4. Global distributions of the multi-model mean and RSD (relative standard deviation) of ratios of BC column burdens in 2000 to these in 1850.

ACPD
12, 21713–21778, 2012

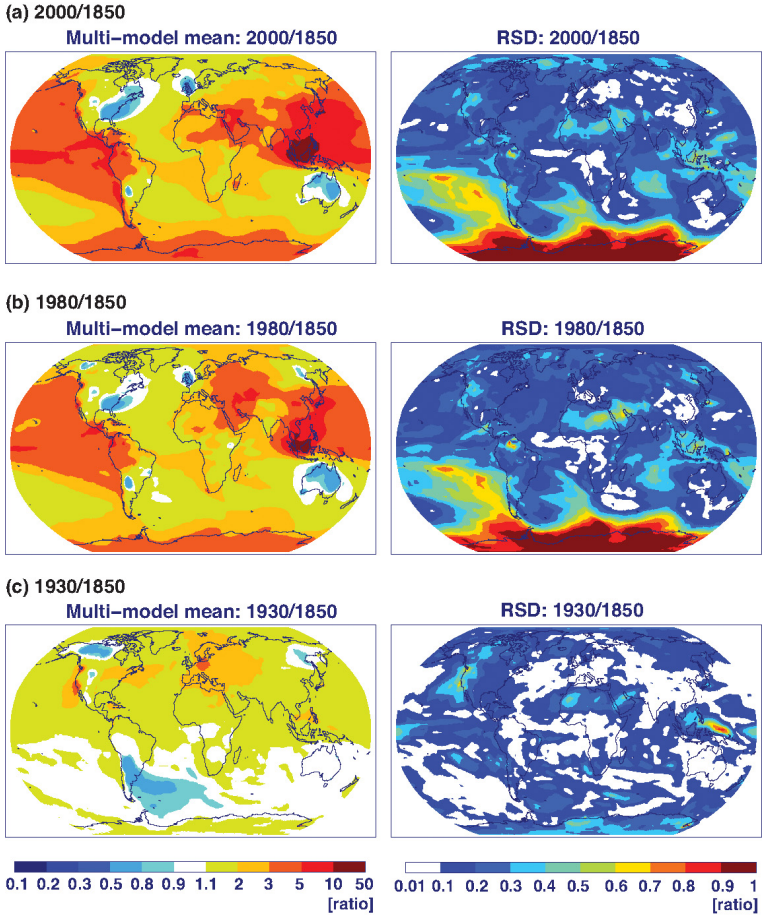

Fig. 5. Global distributions of the multi-model mean and RSD (relative standard deviation) of ratios of total BC deposition fluxes in 2000, 1980, and 1930 to these in 1850.

ACPD
12, 21713–21778, 2012

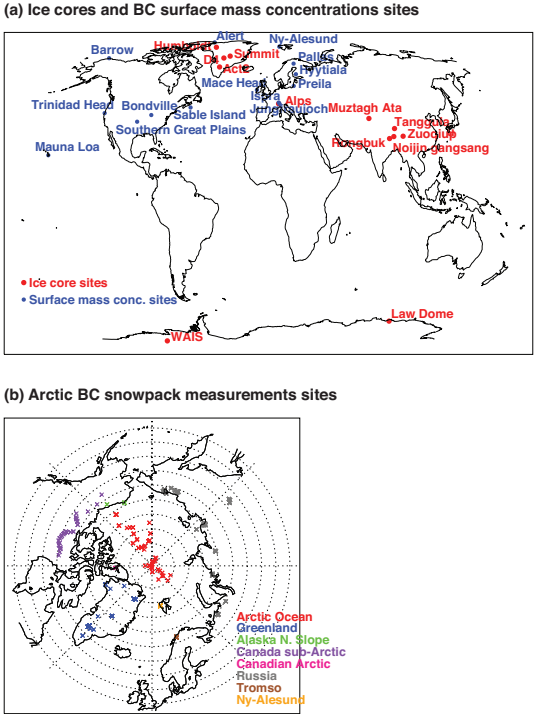

Fig. 6. Geographical locations of **(a)** ice core sites (listed in Table 5) shown in red and atmospheric surface mass concentration sites (listed in Table 4) in blue and **(b)** Arctic BC snow concentrations sites.

ACPD
12, 21713–21778, 2012

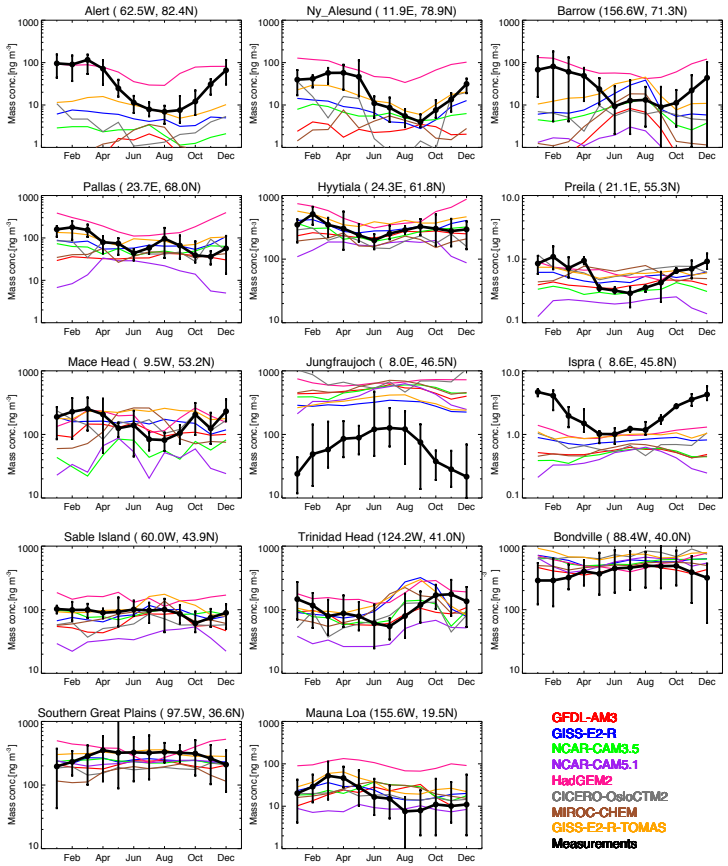

Fig. 7. Seasonal cycle of atmospheric BC surface mass concentrations at the observation sites listed in Table 4. Note that the observed BC is shown with the black line with the error bar including the minimum and maximum monthly mean during the observation period.

ACPD
12, 21713–21778, 2012

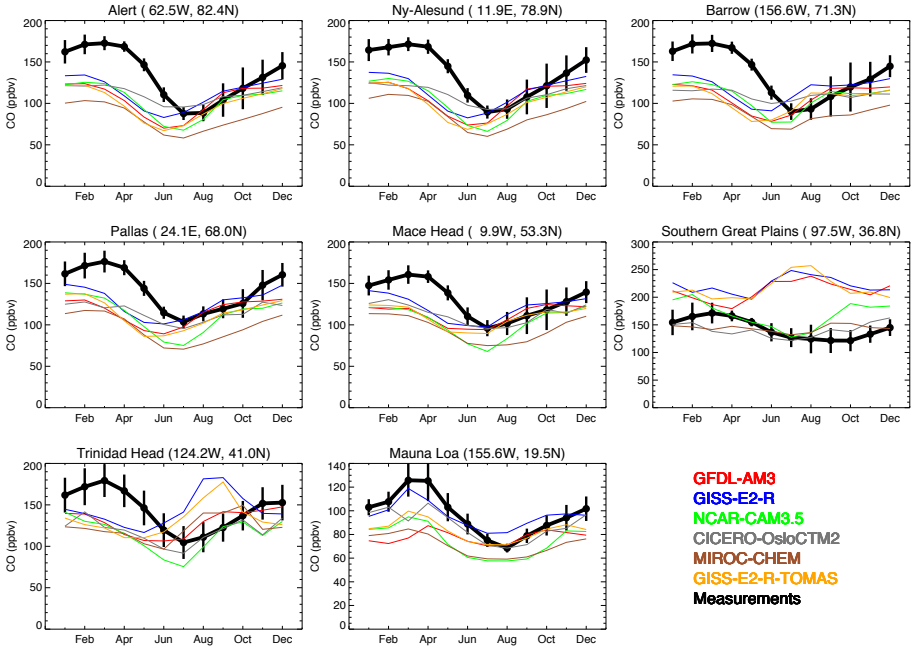

Fig. 8. Same as Fig. 7 but for CO mixing ratio. Note that the stations in Table 4 are excluded if the CO measurements are not available, and the measured CO is averaged with available data between 1996 and 2005. NCAR-CAM5.1 and HadGEM2 do not provide CO output.

ACPD
12, 21713–21778, 2012

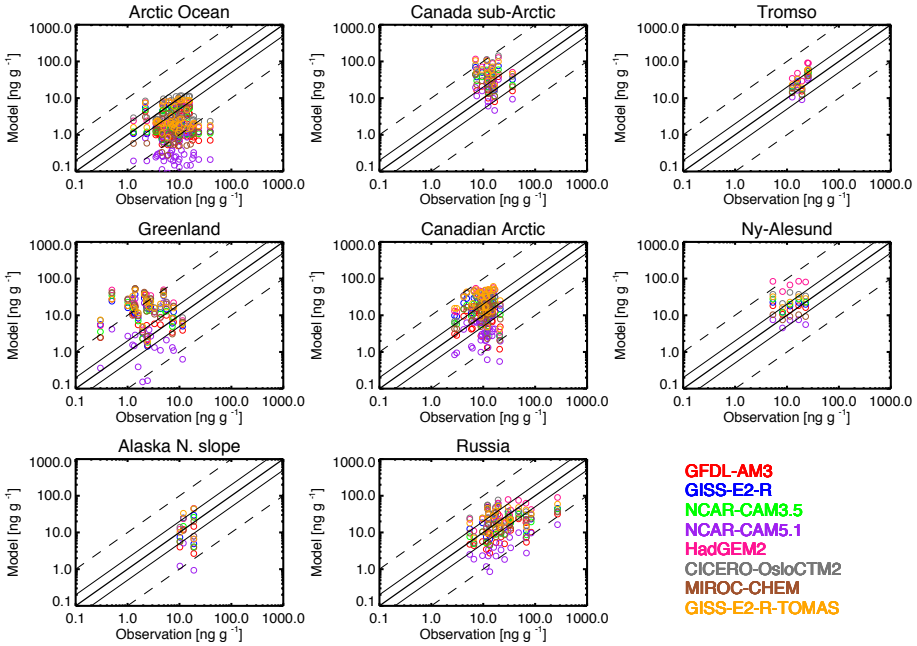

Fig. 9. Scatter plots of the observed Arctic BC snow concentrations from 1998 and 2005–2009 and the modeled BC snow concentrations that were obtained from the offline land and sea-ice models (described in Sect. 3). Refer Sect. 4.3 for the data preparation. The thick and thin solid lines refer to 1 : 1 line and 2 : 1 line, respectively. The dashed line is for 10 : 1 line.

ACPD
12, 21713–21778, 2012

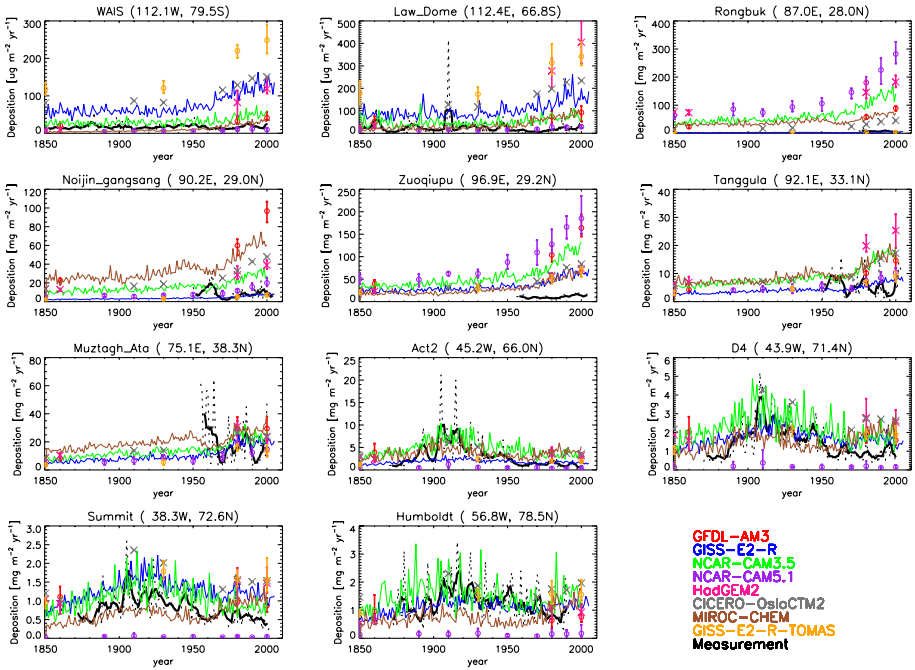

Fig. 10. Comparison of annual-average BC deposition fluxes in models to ice core observations. Observations are shown in two ways: annual-average shown in black dot and 5-yr running average shown in thick black line. Note that the CMIP5 transient simulations for NCAR-CAM3.5 and MIROC-CHEM are used here (presented as a solid line) instead of their ACCMIP timeslice simulations. For models with the timeslice runs, an error bar is used to present the mean of each timeslice runs with its minimum and maximum of the corresponding timeslice runs and are positioned at the beginning of the corresponding timeslice year. CICERO-OsloCTM2 and HadGEM2 is presented with "X" symbol for their mean.

ACPD
12, 21713–21778, 2012

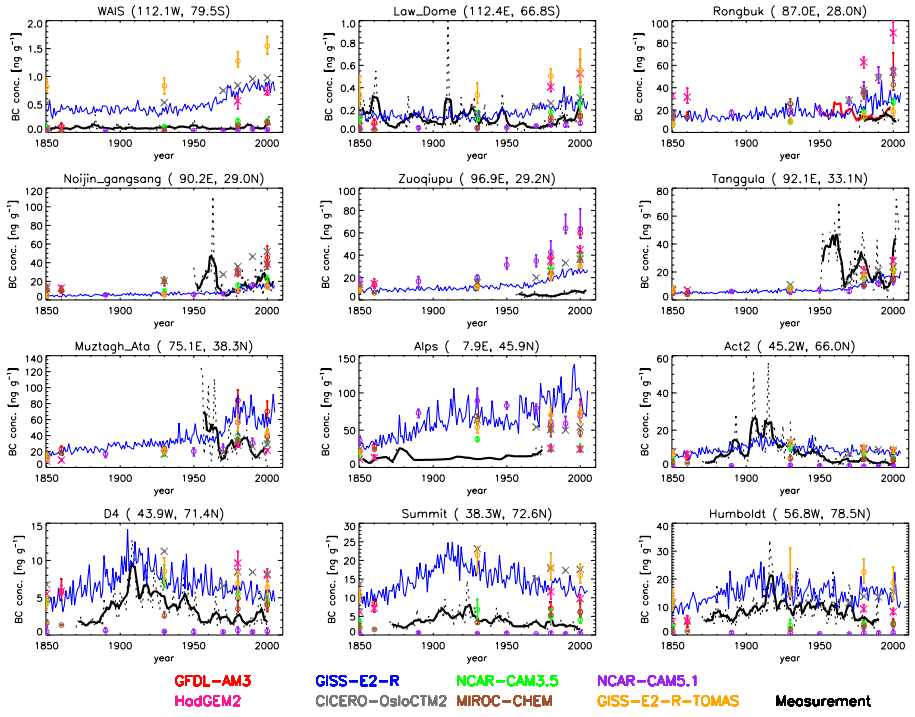

Fig. 11. Same as Fig. 10 but for BC snow concentrations. The red thick line in Rongbuk is BC ice core data from Ming et al. (2008). Note that, unlike Fig. 10, the ACCMIP timeslice simulations for NCAR-CAM3.5 and MIROC-CHEM are used.

ACPD
12, 21713–21778, 2012

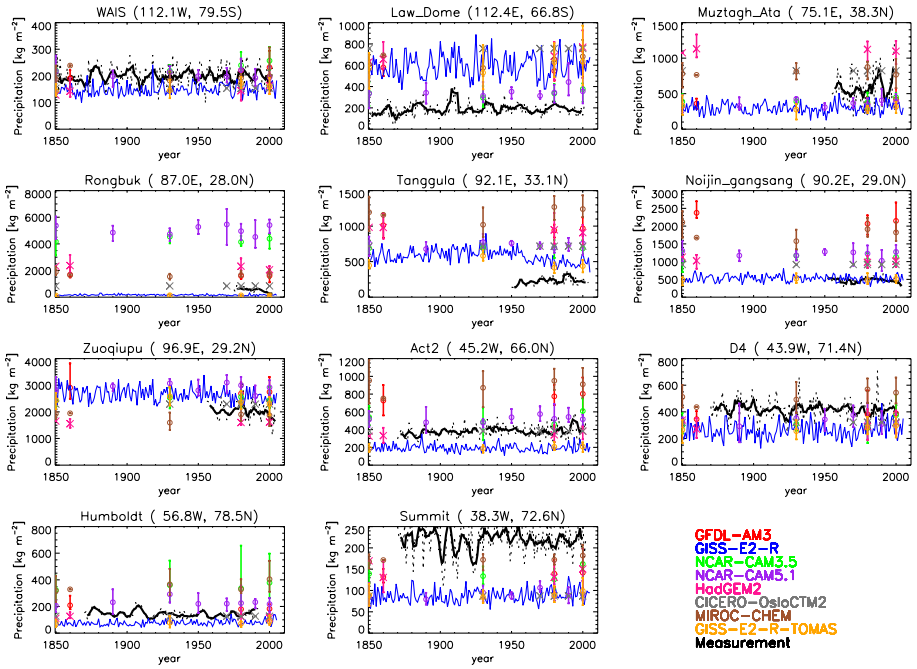

Fig. 12. Same as Fig. 10 but for annually accumulated precipitation ($kg m^{-2}$). The observed precipitation shown here is computed based on the observed BC deposition fluxes divided by the observed BC snow concentration. Note that the ACCMIP timeslice simulations for NCAR-CAM3.5 and MIROC-CHEM are used.

ACPD
12, 21713–21778, 2012

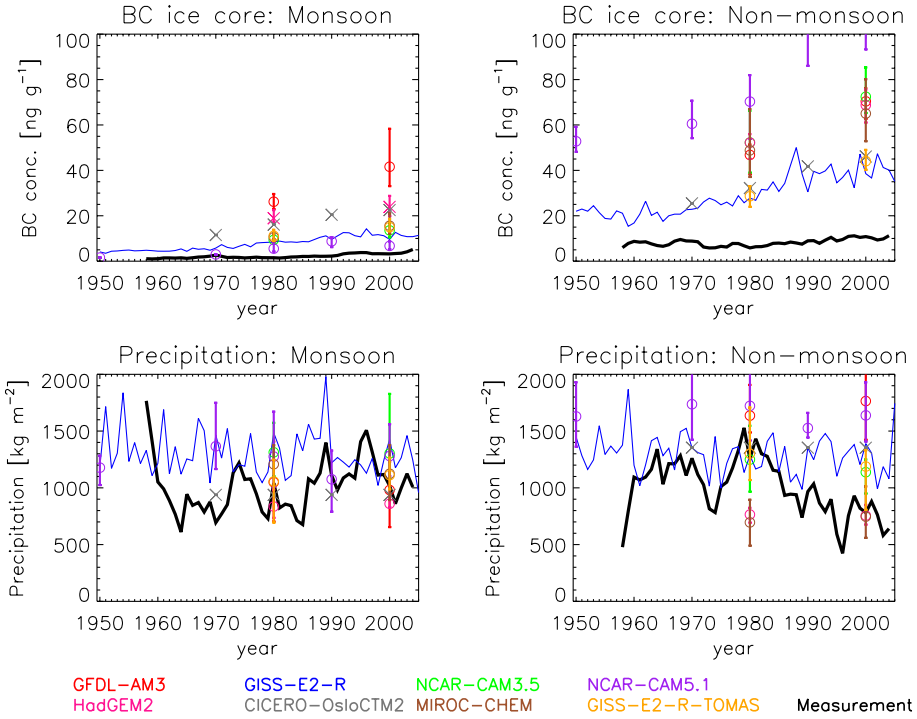

Fig. 13. Temporal trends of 5-yr running average of BC snow concentrations (ng g^{-1}) and accumulated precipitations (kg m^{-2}) during monsoon (June to September) and non-monsoon (October to May) seasons at Zuoqiupu. Refer the color scheme and the plotting method to the caption of Fig. 10 and Sect. 4.4 for how the observed precipitation data is prepared. Note that the ACCMIP timeslice simulations for NCAR-CAM3.5 and MIROC-CHEM are used.

ACPD
12, 21713–21778, 2012

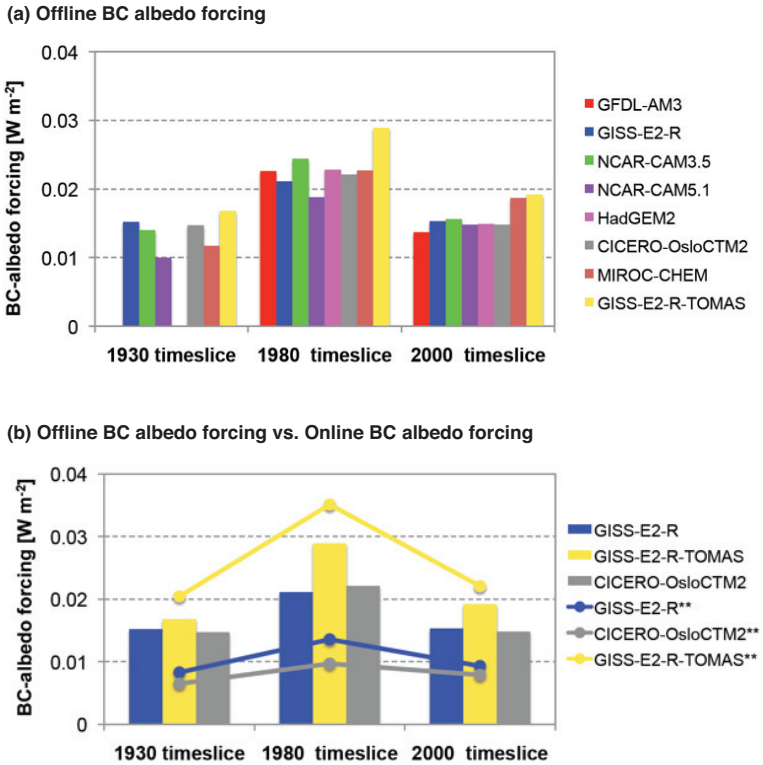

Fig. 14. Global annual average of offline BC albedo forcing from 8 ACCMIP models **(a)** and comparison of the offline forcing to online BC albedo forcing **(b)**. Note that the offline BC albedo forcing is computed in the offline land and sea-ice models (CLM4 and CICE4, see Sect. 3 for more details), and the online BC albedo forcing is computed in its own model. In **(b)**, the offline BC albedo forcing is shown in the bar plot and the online forcing, in the line plot.

ACPD
12, 21713–21778, 2012

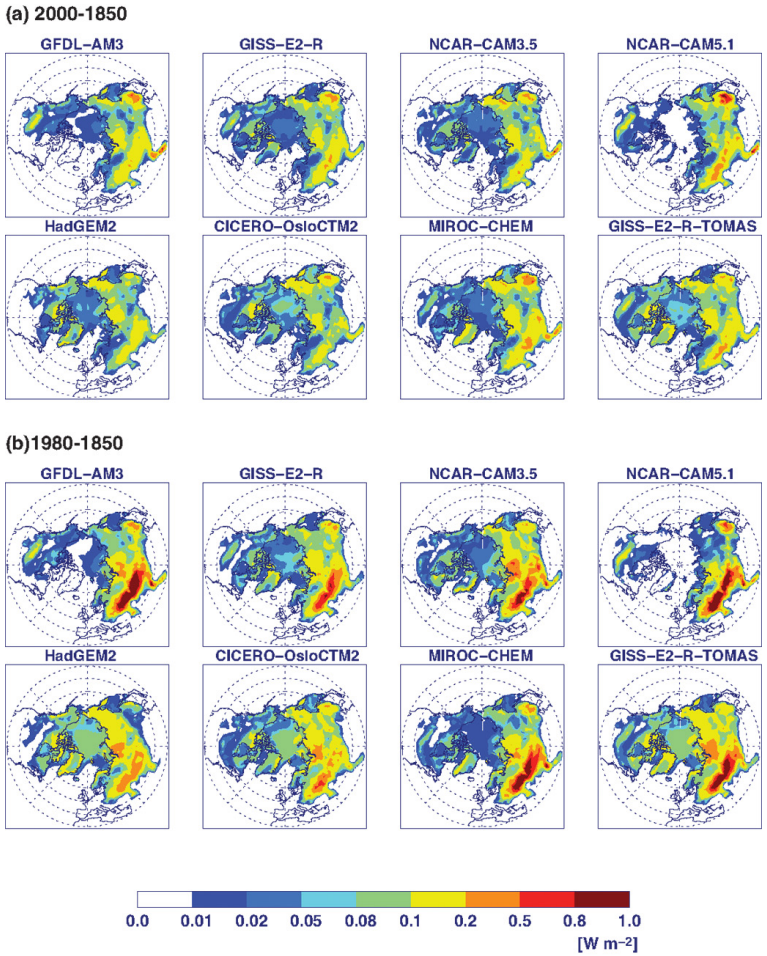

Fig. 15. Global distributions of the offline BC albedo forcing in **(a)** 2000 relative to 1850 and **(b)** 1980 relative to 1850.

ACPD
12, 21713–21778, 2012